TKK Dissertations 39
Espoo 2006

NOVEL SENSOR AND TELECOMMUNICATION APPLICATIONS OF PHOTONIC CRYSTAL FIBERS

Doctoral Dissertation

Tuomo Ritari

Helsinki University of Technology
Department of Electrical and Communications Engineering
Optics and Molecular Materials

TKK Dissertations 39
Espoo 2006

NOVEL SENSOR AND TELECOMMUNICATION APPLICATIONS OF PHOTONIC CRYSTAL FIBERS

Doctoral Dissertation

Tuomo Ritari

Dissertation for the degree of Doctor of Science in Technology to be presented with due permission of the Department of Electrical and Communications Engineering for public examination and debate in Micronova at Helsinki University of Technology (Espoo, Finland) on the 4th of August, 2006, at 12 noon.

Helsinki University of Technology
Department of Electrical and Communications Engineering
Optics and Molecular Materials

Teknillinen korkeakoulu
Sähkö- ja tietoliikennetekniikan osasto
Optiikka ja molekyylimateriaalit

Distribution:
Helsinki University of Technology
Department of Electrical and Communications Engineering
Optics and Molecular Materials
P.O. Box 3500
FI - 02015 TKK
FINLAND
URL: http://omm.tkk.fi/
Tel. +358-9-4511
Fax +358-9-451 3128
E-mail: Tuomo.Ritari@tkk.fi

ISBN 951-22-8298-4
ISBN 951-22-8299-2 (PDF)
ISSN 1795-2239
ISSN 1795-4584 (PDF)
URL: http://lib.tkk.fi/Diss/2006/isbn9512282992/

TKK-DISS-2163

Otamedia Oy
Espoo 2006

HELSINKI UNIVERSITY OF TECHNOLOGY P. O. BOX 1000, FI-02015 TKK http://www.tkk.fi	ABSTRACT OF DOCTORAL DISSERTATION

Author Tuomo Matias Ritari

Name of the dissertation

Novel sensor and telecommunication applications of photonic crystal fibers

Date of manuscript March 20, 2006	Date of the dissertation August 4, 2006
☐ Monograph	☒ Article dissertation (summary + original articles)

Department	Electrical and Communications Engineering
Laboratory	Optics and Molecular Materials
Field of research	Optical technology
Opponent	Tim Birks, Professor
Supervisor	Hanne Ludvigsen, Docent

Abstract

Photonic crystal fibers are novel optical waveguides containing a periodic array of air holes running along the fiber around a solid or hollow core. These fibers have recently attracted great interest in many research areas such as in nonlinear optics and measurement science as their manufacturing process allows for a high flexibility in the fiber design. Index-guiding photonic crystal fibers are commonly referred to as microstructured fibers whereas hollow-core photonic crystal fibers which guide light through a photonic bandgap effect are called photonic bandgap fibers. The thesis provides results on the polarization properties of microstructured fibers and presents novel applications which utilize both the unique physical structure and optical characteristics of microstructured and photonic bandgap fibers.

Polarization effects can have a great impact on the operation of fiber-based devices and communication systems. In particular, polarization-mode dispersion can limit long distance high bit-rate data transmission. In this thesis, the polarization characteristics of microstructured fibers and the sensitivity of these properties to the temperature and wavelength are studied. Also, polarization-mode dispersion of large mode-area microstructured fibers is investigated.

One of the earliest applications of microstructured fibers is supercontinuum generation. In the thesis, supercontinuum generation is studied in large mode-area microstructured fibers by employing nanosecond laser pulses. The special properties of these fibers allow for the realization of single-mode supercontinuum sources with a high spectral density, low output beam divergence and low polarization dependence. Moreover, a novel nanosecond supercontinuum source based on an acetylene-filled nonlinear microstructured fiber is presented. The approach provides a broadband source that is self-referenced to the absorption lines of the gas.

Air-guiding photonic bandgap fibers can guide more than 98% of the light in air thus reducing the influence of the material parameters of silica on the optical properties of the fiber. By filling the fiber holes with gas, such a fiber can provide a very long optical path length in compact fashion. In this thesis, the use of photonic bandgap fibers in gas sensing is studied. The high sensitivity and long interaction length provided by PBFs allows for the detection of molecules with weak absorption lines. In addition, a compact optical wavelength reference based on a gas-filled photonic bandgap fiber is presented. By utilizing lock-in technique, the output frequency of the laser was stabilized to the center point of weak acetylene absorption lines coinciding with wavelength division multiplexing channels.

Keywords photonic crystal fiber, polarization-mode dispersion, supercontinuum, gas detection, wavelength reference

ISBN (printed) 951-22-8298-4	ISSN (printed) 1795-2239
ISBN (pdf) 951-22-8299-2	ISSN (pdf) 1795-4584
ISBN (others)	Number of pages 110

Publisher Optics and Molecular Materials, Department of Electrical and Communications Engineering

Print distribution Optics and Molecular Materials, Department of Electrical and Communications Engineering

☒ The dissertation can be read at http://lib.tkk.fi/Diss/2006/isbn9512282992/

TEKNILLINEN KORKEAKOULU PL 1000, 02015 TKK http://www.tkk.fi	VÄITÖSKIRJAN TIIVISTELMÄ

Tekijä Tuomo Matias Ritari

Väitöskirjan nimi

Fotonikidukuitujen sovellukset anturi- ja tietoliikennetekniikassa

Käsikirjoituksen jättämispäivämäärä 20.3.2006	Väitöstilaisuuden ajankohta 4.8.2006
☐ Monografia	☒ Yhdistelmäväitöskirja (yhteenveto + erillisartikkelit)

Osasto	Sähkö- ja tietoliikennetekniikan osasto
Laboratorio	Optiikka ja molekyylimateriaalit
Tutkimusala	Optinen teknologia
Vastaväittäjä	Prof. Tim Birks
Työn valvoja	Dos. Hanne Ludvigsen

Tiivistelmä

Fotonikidekuidut ovat uudenlaisia optisia aaltojohteita, joissa on kiinteän tai onton ytimen ympärillä kuidun pituussuunnassa kulkevia ilmareikiä. Muuttamalla reikien määrää, kokoa ja sijaintia voidaan säädellä tarkasti kuitujen ominaisuuksia. Tämä väitöskirja käsittelee fotonikidekuitujen ominaisuuksia sekä kuituihin perustuvia sovelluksia.

Valon polarisaatiolla on suuri vaikutus valokuitua hyödyntävien laitteiden ja optisten tiedonsiirtojärjestelmien toimintaan. Erityisesti, optisissa kuiduissa esiintyvä polarisaatiomuotodispersio rajoittaa tiedonsiirtoa nopeissa optisissa tietoliikennejärjestelmissä. Tässä työssä tutkitaan fotonikidekuitujen polarisaatio-ominaisuuksia sekä näiden ominaisuuksien herkkyyttä lämpötilalle. Lisäksi työssä tarkastellaan fotonikidekuitujen polarisaatiomuotodispersiota.

Työssä tutkitaan myös valkoisen laajakaistaisen valon muodostumista suuriytimisissä sekä epälineaarisissa fotonikidekuiduissa kytkemällä kuituihin nanosekuntilaserpulsseja. Suuriytimiset kuidut mahdollistavat yksimuotoisen, suuritehoisen valkoisen valon valonlähteen kehittämisen. Lisäksi tällaisen valonlähteen etuja ovat pieni ulostulosäteen divergenssi sekä polarisaatioriippuvuus. Epälineaarisissa fotonikidekuiduissa osa valosta kulkee kuidun rei'issä, jotka voidaan täyttää valoa absorboivilla kaasuilla. Työssä tarkastellaan myös epälineaarisen kuidun käyttöä samanaikaisesti sekä kaasukennona että laajakaistaisena valonlähteenä kytkemällä kaasulla täytettyyn kuituun nanosekuntilaserpulsseja.

Onttoytimisissä fotonikidekuiduissa yli 98% valosta voi edetä ontossa ytimessä. Ontto ydin voidaan täyttää kaasuilla tai nesteillä, mikä antaa mahdollisuuden käyttää kuituja erilaisina antureina, referensseinä ja kytkiminä. Työssä sovelletaan onttoytimisiä kuituja kaasujen absorptiomittaukseen. Ainutlaatuisen rakenteensa vuoksi kuiduilla voidaan saavuttaa pitkä vuorovaikutusmatka valon ja kaasun välillä. Lisäksi työssä kehitetään onttoytimiseen kuituun perustuva aallonpituusreferenssi. Kaasulla täytetty kuitu tarjoaa pienikokoisen valon absorptioon perustuvan referenssin. Työssä tutkitaan erityisesti tällaisen referenssin soveltuvuutta aallonpituuskanavointia hyödyntäviin tietoliikennejärjestelmiin.

Asiasanat fotonikidekuitu, polarisaatiomuotodispersio, superkontinuumi, kaasujen havainnointi, aallonpituusreferenssi

ISBN (painettu)	951-22-8298-4	ISSN (painettu)	1795-2239
ISBN (pdf)	951-22-8299-2	ISSN (pdf)	1795-4584
ISBN (muut)		Sivumäärä	110

Julkaisija Optiikka ja molekyylimateriaalit, Sähkö- ja tietoliikennetekniikan osasto

Painetun väitöskirjan jakelu Optiikka ja molekyylimateriaalit, Sähkö- ja tietoliikennetekniikan osasto

☒ Luettavissa verkossa osoitteessa http://lib.tkk.fi/Diss/2006/isbn9512282992/

Preface

The research for this thesis has been carried out within the Fiber-Optics Group in the laboratory of Optics and Molecular Materials, Helsinki University of Technology, during the years 2002-2005. I would like to express my gratitude to Hanne Ludvigsen for providing me the opportunity to work within the laboratory and for raising funding and arranging visits abroad. I am also grateful for her supervision throughout the course of the thesis.

Furthermore, I would like to thank my co-workers Jesse Tuominen, Goëry Genty and Tapio Niemi who have worked with me in many projects and provided a great deal of help. I would also like to thank Mikko Lehtonen for many stimulating discussions and badminton games.

In addition, I would like to express my warmest thanks to Dr. Jan C. Petersen for lending his lab at Danish Fundamental Metrology and for sharing his long time experience in molecular spectroscopy. Dr. Mark Wegmuller is acknowledged for providing me the opportunity to visit Geneva University and for sharing his knowledge in polarization measurement techniques. Dr. Jacob Folkenberg is acknowledged for sharing his knowledge of photonic crystal fibers. Crystal Fibre A/S kindly provided the fiber samples used in the work conducted within the COST 265 and COST P11 Actions.

I am also very thankful for Prof. Nicolas Gisin and Matthieu Legré of the Group of Applied Physics at Geneva University and Anders Bjarklev, Theis Hansen and Thorkild Sørensen at the Research Centre COM in Denmark. Also, I would like to thank all the other co-authors of the publications for their contribution. Esa Räikkönen and Scott Buchter are acknowledged for help with the nanosecond Nd:YAG laser. I am also very thankful for the pre-examiners Ole Bang and Rolf Hernberg for their valuable comments.

The funding of this work has been provided by the Graduate School on Modern Optics and Photonics and the Academy of Finland (project no: 121117, 120777). A three-month visit in Denmark during Autumn 2003 and Spring 2004 was financed by Nordforsk. A one-month visit in Switzerland in Summer 2004 was a Short Term Scientific Mission within the COST Action P11. NKT Research is acknowledged for providing some of the fiber samples. Nokia Foundation, Emil Aaltonen Foundation and Suomen Kulttuurirahasto are also acknowledged for the funding of this work.

Most of all, I would like to thank my wife Anne for her love and patience and also my whole family for their endless support.

Espoo, March 20, 2006

Tuomo Ritari

Table of contents

List of Publications

This dissertation consists of an overview and the following six publications:

[P1] T. Ritari, M. Wegmuller, M. Legré, N. Gisin, J. R. Folkenberg, M. D. Nielsen, and H. Ludvigsen, "Experimental study of polarization properties of highly birefringent photonic crystal fibers", *Opt. Express* **12**, 5931-5939 (2004).

[P2] T. Ritari, T. Niemi, M. Wegmuller, N. Gisin, J. R. Folkenberg, A. Pettersson, and H. Ludvigsen, "Polarization-mode dispersion of large mode-area photonic crystal fibers", *Opt. Commun.* **226**, 233-239 (2003).

[P3] G. Genty, T. Ritari, and H. Ludvigsen, "Supercontinuum generation in large mode-area microstructured fibers", *Opt. Express* **13**, 8625-8633 (2005).

[P4] T. Ritari, G. Genty, and H. Ludvigsen, "Supercontinuum and gas cell in a single microstructured fiber", *Opt. Lett.* **30**, 3380-3382 (2005).

[P5] T. Ritari, J. Tuominen, J. C. Petersen, T. Sørensen, T. P. Hansen, H. Simonsen, and H. Ludvigsen, "Gas sensing using air-guiding photonic bandgap fibers", *Opt. Express* **12**, 4080-4087 (2004).

[P6] J. Tuominen, T. Ritari, J. C. Petersen, and H. Ludvigsen, "Gas-filled photonic bandgap fibers as wavelength references", *Opt. Commun.* **255**, 272-277 (2005).

The references to these papers will be denoted by P1-P6.

Author's Contribution

The scientific results presented in this dissertation have been carried out within the Fiber-Optics Group in the laboratory of Optics and Molecular Materials during the years 2002-2005. Part of the research work is an outcome of collaboration with research groups in Denmark and Switzerland. The dissertation consists of a short overview and six publications referred to as P1-P6. All the publications are the results of team work. The author has written the manuscripts of papers P2, P4 and P5, the final version of the manuscript of paper P1, prepared a part of the manuscript of paper P6 and contributed to the preparation of paper P3. The results reported have also been presented by him in several international conferences.

For paper P1, the author carried out the measurements performed at Helsinki University of Technology. He visited the Group of Applied Physics at Geneva University for one month to conduct part of the experiments there and contributed to the analysis of the measurement results. For paper P2, the author constructed the measurement setup and carried out most of the measurements conducted at Helsinki University of Technology. Also he contributed to the analysis of the measurement results. The author participated in the experiments and contributed to the analysis of the results presented in papers P3 and P4. Part of the experimental setup employed in the latter of these papers was constructed by him. The work of paper P5 was started during a three-month stay in autumn 2003 at the institute of Danish Fundamental Metrology (DFM) in Denmark and the measurement session was finalized during another one-month stay in spring 2004 at DFM. The author planned the measurement setup prior to the stay and he was the driving force throughout the whole course of the work. He carried out most of the measurements and conducted the main part of the analysis of the measurement results. For paper P6, the author participated in the experiments and the analysis of the measurement results.

Other related publications to which the author has contributed

*T. Ritari, H. Ludvigsen, and J. C. Petersen, "Photonic bandgap fibers in gas detection", Spectroscopy **20** (4), 30-33 (2005).*

1 Introduction

The development of photonic crystal fibers (PCFs) and their large number of potential applications have attracted a lot of interest since the middle of the nineties [1]. Photonic crystal fibers are commonly referred to as microstructured fibers (MFs), microstructured optical fibers (MOFs) or holey fibers (HFs). The word microstructure refers to the cross-sectional structure of the fiber that typically consists of a periodic high-index contrast structure of silica and air on the length scale of the wavelength. The aforementioned terms are often used to describe an index-guiding PCF in which light is confined to a high-index core surrounded by an air-silica cladding with a lower effective refractive index. Another type of PCF is called photonic bandgap fiber (PBF). These fibers guide light in a low-index core through the photonic bandgap effect [2, 3].

The unique manufacturing technology of PCFs allows for the precise tuning of the optical properties by changing the size, shape and position of the cladding holes. Photonic crystal fibers provide extraordinary dispersion properties [4], endlessly single-mode guidance [5], light guidance in air [6], an order of magnitude higher birefringence [7] and enhanced nonlinear effects [8] compared with conventional optical fibers. These special properties have led to the development of several applications in the fields of optical communications [9, 10], nonlinear optics [8, 11], sensing [12-15], high power technology [16] and optical metrology [17]. In particular, the presence of air holes in the fiber structure and the use of single fabrication material are useful, e.g., in many sensing and interferometric applications.

Optical fibers always exhibit small birefringence due to mechanical stress even if they have a circularly symmetric design. Birefringence is usually an undesirable property of optical fibers. Nevertheless, in many sensing applications and in applications requiring light to maintain a linear polarization state, a high level of birefringence is often desired. In order to build reliable fiber-based sensors and devices it is also important to consider the influence of environmental factors on the fiber characteristics. In particular, when high temperature variations are present, temperature effects may limit the operation of, e.g., fiber-optic gyroscopes and polarimetric sensors. Photonic crystal fibers could be good candidates for applications requiring high, temperature insensitive, birefringence. The high refractive index contrast between silica and air and the possibility of introducing large asymmetries in the PCF structure can be exploited to provide strong form birefringence [7]. Moreover, the use of single fabrication material alleviates the constraints caused by the thermal and mechanical incompatibility of different solid materials. On the other hand, large-mode area PCFs with stress applying elements could be employed in polarization-maintaining high-power applications requiring single-mode operation. In order to find out the suitability of PCFs for, e.g., sensing applications, an accurate characterization of birefringence properties has to be performed.

Large mode-area (LMA) PCFs [18] are particularly suitable for high-power applications. Furthermore, LMA-PCFs may prove to be useful in optical communications due to their endlessly single-mode operation and low nonlinearity. In contrast to sensing applications, fibers used in optical communications require low values of birefringence and polarization-mode dispersion (PMD). Polarization-mode dispersion is related to the random behavior of birefringence in optical fibers and is one of the main limitations on the data transmission rate in high bit-rate communication systems operating over long distances. In order for the LMA-PCFs to be useful in telecommunication applications, the polarization characteristics of such

fibers need to be carefully investigated. Moreover, as the optical and mechanical properties of PCFs differ from conventional optical fibers, the suitability of standard measurement techniques has to be assessed in the case of PCFs.

One of the earliest applications of PCFs is supercontinuum (SC) generation [8]. When temporally short high power pulses are coupled into a nonlinear medium, the bandwidth of the pulses can experience substantial spectral broadening. The small mode areas available with PCFs together with the special dispersion properties have allowed for significant increase of the SC bandwidth. In some applications, however, properties such as high spectral power density could be desired. The power limitation encountered in narrow-core PCFs due to the strong field confinement can be alleviated by employing LMA-PCFs. These fibers also provide the advantage of being truly single mode at all wavelengths and exhibit a small numerical aperture resulting in a small output beam divergence. Although their nonlinearity is much lower compared to narrow-core PCFs, LMA-PCFs typically exhibit smaller OH-losses and, thus, allow for the use of longer fiber lengths to compensate for the lower nonlinearity. Supercontinuum light sources find applications in optical frequency metrology [17], characterization of optical components [19, 20], optical coherence tomography [21, 22] and in optical communications [23].

The unique microstructure of PCFs can be exploited in sensing applications [12-15]. By filling the holes of index-guiding narrow-core PCFs with gases, molecular species can be detected via evanescent-field effects using absorption spectroscopy [14]. Apart from sensing, this special property can be utilized to develop novel light sources. By exploiting both the evanescent-field effect and the high nonlinearity of narrow-core PCFs, it is possible to combine a broadband light source and a reference gas cell in a single PCF. Such sources could find applications for instance in broadband characterization of optical components and in calibration of measurement devices.

Air-guiding PBFs [6] allow for a substantial improvement in the overlap between the guided mode and the gas compared with index-guiding PCFs, thereby, reducing considerably the length of the fiber needed. Such fibers are, therefore, better suited for gas sensing applications. Gas-filled photonic bandgap fibers provide also a possibility for realizing compact optical wavelength references. With the long natural interaction length of the PBF, weak absorption lines can be used without the need for cumbersome multi-pass absorption cells. Photonic bandgap fiber based references may find applications in calibration of optical measurement instruments and in monitoring channel wavelengths in wavelength division multiplexing (WDM) systems.

In addition to an introduction to PCFs, the thesis consists of three parts. In the first part, the polarization properties of both birefringent narrow-core PCFs and LMA-PCFs are investigated. Furthermore, the temperature and wavelength dependence of the polarization characteristics is discussed. The second part deals with SC generation in LMA-PCFs and narrow-core PCFs using nanosecond laser pulses. The last part concentrates on gas spectroscopy applications employing PCFs.

2 Photonic crystal fibers

Photonic crystal fibers are novel optical waveguides that possess a periodic microstructured cladding around a solid or hollow core in the plane perpendicular to the fiber axis. Due to their unique geometrical structure, these fibers can exhibit a large number of optical properties not obtainable in conventional optical fibers. In this Chapter, the history, classification, fabrication and optical properties of PCFs are shortly discussed.

2.1 History

The idea of producing optical fibers from single low-loss material dates back to 1970's when Kaiser *et al.* reported the fabrication of microstructured air-silica optical fibers at Bell Laboratories [24]. The motivation for this work originated from the belief that the doping of the fiber core would cause undesirable effects such as stress at the cladding-core interface and would also limit the minimum attainable fiber loss [25]. Due to the technological development of doped optical fibers mainly within the area of optical communications, the single-material fibers were not developed much further. The tremendous progress of PCFs took place only during the last decade when the manufacturing technology (e.g. stack-and-draw method) was advanced enough to allow for the precise fabrication of complex silica-air structures [1]. In 1995, Russell and co-workers proposed an optical fiber that would guide light in a hollow core using a photonic bandgap cladding [26, 27]. One year later, in 1996, the first index-guiding PCF with a periodic air-silica cladding structure was presented [1]. This was followed by the first experimental demonstration of a PBF with a honeycomb lattice in 1998 [28]. In such a fiber, light is guided in a core which has a lower effective refractive index than the cladding. In the honeycomb design, the majority of the mode energy is still located in silica. In 1999, the first air-guiding PBF with a triangular cladding structure was introduced [6]. Such fibers can guide more than 98% of the power in the air-regions of the fiber. Some important development steps and applications of PCFs are listed on Table 1.

Table 1. Important development steps of photonic crystal fibers.

Year	Milestones
1973	Microstructured air-silica optical fiber [24]
1987	Idea of photonic bandgap structure [2, 3]
1995	Hollow-core fiber with photonic bandgap cladding proposed [26]
1996	First demonstration of a MF with a periodic air-silica cladding [1]
1998	First demonstration of a photonic bandgap fiber [28]
1998	Large mode area microstructured fiber [18]
1999	Air-guiding photonic bandgap fiber [6]
1999	Supercontinuum generation in a microstructured fiber [8]
2000	Highly birefringent microstructured fiber [7]

2.2 Classification

Photonic crystal fibers can be divided into two classes, index-guiding fibers [1, 27] and bandgap-guiding fibers [6, 27, 28], based on the light guiding mechanisms. The classification is presented in Fig. 1 and the different guiding mechanisms are illustrated in Fig. 2. Silica (n≈1.45) is most commonly used as the fabrication material of PCFs.

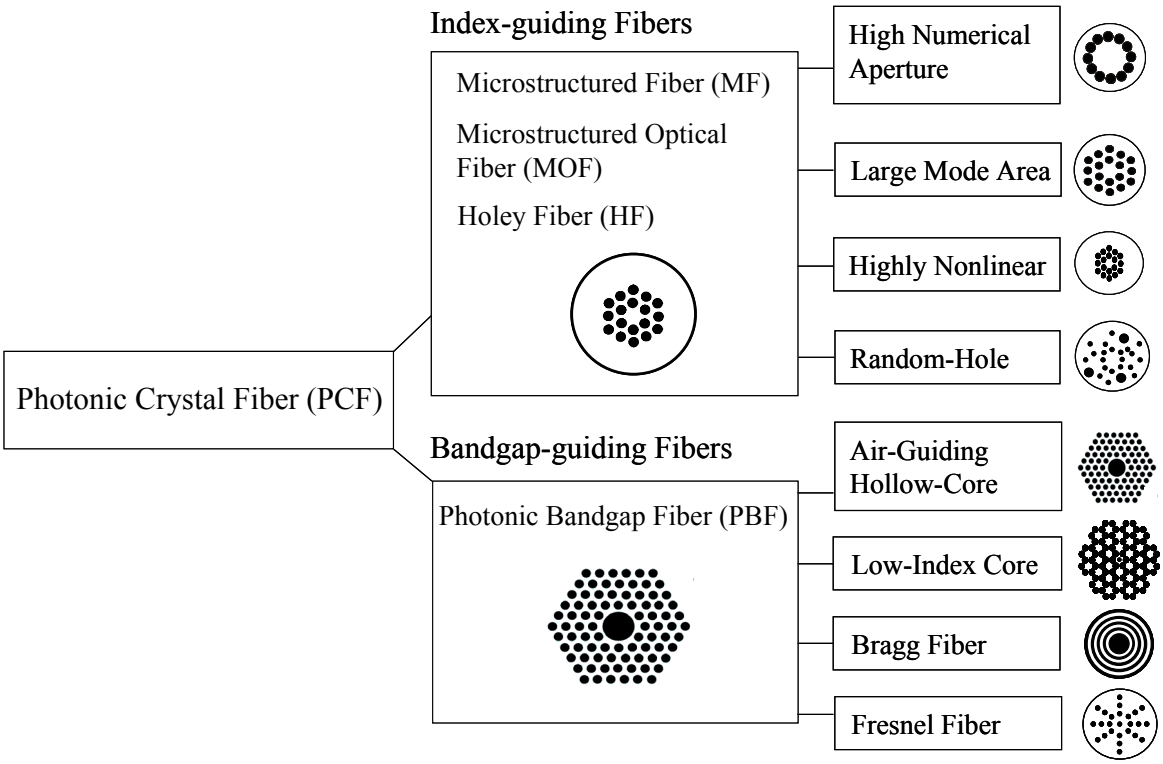

Figure 1. Classification of photonic crystal fibers [25].

The main classes can be further divided into several subclasses on the grounds of the fiber structure and the optical properties. Index-guiding PCFs have a solid core and a periodic [1] or a random arrangement [29] of air holes in the fiber cladding. The air holes lower the effective refractive index of the cladding compared with that of the solid core. This allows for the light to be guided by total internal reflection as in conventional optical fibers (see Fig. 2a). The second class of PCFs is referred to as photonic bandgap fibers. In the case of the PBF, the periodic cladding microstructure results in a photonic bandgap that confines light inside a hollow core or in a core made of material with a refractive index lower than that of the effective index of the cladding. As a consequence, light can be guided in a gas-filled core [6, 11] or even in a solid core [30]. The bandgap is a result of multiple Bragg reflections [6], which leads to the wavelength dependence of light transmission (see Fig. 2b). The fabrication and optical properties of both PCF types are discussed in the following sections.

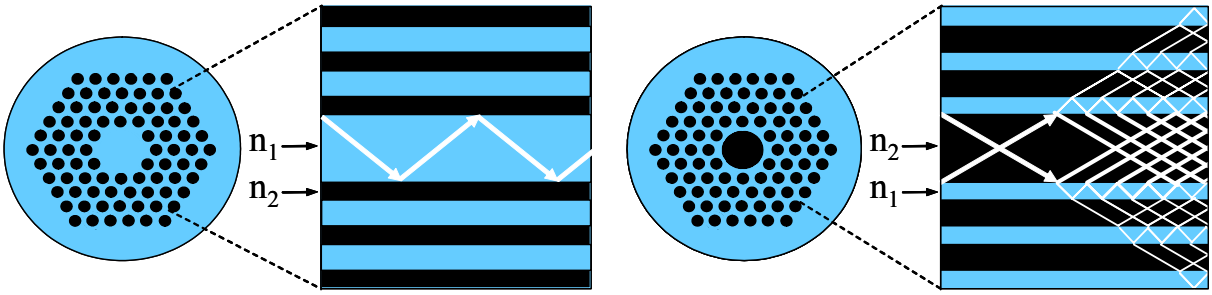

Figure 2. a) Index-guidance, n_1=1.45 (silica) and n_2=1 (air). b) Bandgap-guidance, n_1=1.45 (silica) and n_2=1 (air).

2.3 Fabrication

Photonic crystal fibers are usually manufactured from silica by employing a so-called stack-and-draw method [1, 25] that typically consists of three steps. The first step, the fabrication of a preform, differs from the manufacturing process of a conventional optical fiber using, e.g., a modified chemical vapor deposition technique [31]. In the case of PCFs, the preform is fabricated by stacking silica capillaries or rods to form the desired fiber structure. A preform of an air-guiding PBF can be manufactured by removing 4 [32], 7 [33, 34], 19 [6, 35] or 37 [36] silica tubes from the center of the preform whereas in the case of an index-guiding PCF the core is typically formed by replacing one of the capillaries with a silica rod. After the preform is made, it is drawn to a number of canes that can be employed to produce different sized fibers. Subsequently, a cane is drawn to the final fiber length using a drawing tower while maintaining the initial structure [25, 27]. To avoid the collapse of the air holes, the drawing temperature of silica PCFs (~1900 °C) is slightly lower compared with the one (~2000 °C) used for conventional silica fibers. Usually, a polymer jacket is inserted on the outer surface of the fiber in the end of the manufacturing process to give strength and add mechanical flexibility. A schematic picture of the fabrication process of an air-guiding PBF is shown in Fig. 3.

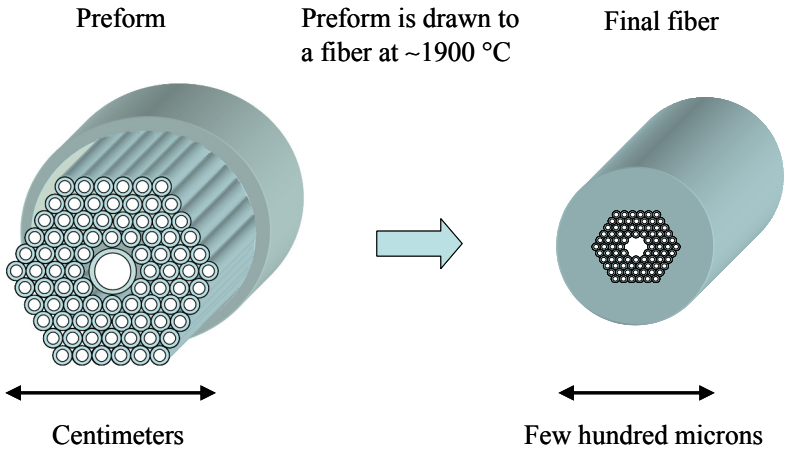

Figure 3. Schematic picture presenting the fabrication process of an air-guiding PBF.

The stack-and-draw method provides high design flexibility. The technique allows for an accurate design of the core shape and size (~1-50 µm) and gives a precise control over the refractive index profile of the cladding. This is particularly important to obtain the desired dispersion, nonlinear and polarization properties. Photonic crystal fibers can also be manufactured from compound glasses by employing an extrusion technique or from

polymers by capillary stacking method, extrusion, casting or injection molding [25, 37-47]. Compared with silica, soft glasses can provide a higher refractive index and nonlinearity, a lower fabrication temperature and a broader spectral operation range.

2.4 Optical properties

Microstructured fibers have received significant attention due to their unique optical properties. More specifically, such fibers can provide special dispersion properties [4], enhanced nonlinearity [8] and higher birefringence compared with conventional optical fibers [7, 48]. Furthermore, the possibility of guiding light in air makes PBFs attractive for many sensing applications. The main optical characteristics of PCFs are shortly described below.

Transmission loss

The rapid development of the PCF manufacturing process over the past few years has led to a considerable improvement in the transmission characteristics of the fibers. Fiber loss can be reduced by enhancing the structural uniformity of the fiber in both transversal and longitudinal direction as well as by reducing material contamination and the surface roughness of the holes. The loss of the state-of-the-art index-guiding PCFs is 0.28 dB/km at 1550 nm [49] whereas conventional single-mode fibers (SMFs) exhibit a loss of less than 0.2 dB/km at 1550 nm. Air-guiding PBFs have potential to exhibit even lower losses than SMFs as most of the light is guided in an air core and, therefore, losses are not limited by Rayleigh scattering and silica absorption in the same way as in conventional optical fibers [35, 50-52]. A loss of 1.2 dB/km at 1620 nm has been reported for a 19-cell PBF [35] and a loss of 13 dB/km at 1500 nm for a 7-cell PBF [33]. Although, the loss is still much higher when compared with the loss of SMFs, the pace of the loss reduction has been very fast for PBFs. In PBFs, losses are mainly caused by leakage loss, light scattering and coupling to surface and cladding modes while the limiting loss mechanism is surface capillary waves [35]. In addition to optical communications, the relatively low loss of PBFs could be beneficial in sensing applications requiring long optical path lengths.

Dispersion

Material dispersion refers to the wavelength dependence of the refractive index of material caused by the interaction between the light and ions, molecules or electrons in material [31, 50, 53]. Apart from material dispersion, another important dispersion type in optical fibers is waveguide dispersion [31, 50, 53]. Waveguide dispersion depends among others on the core diameter and on the refractive index contrast between the core and the cladding. Generally, conventional optical fibers have dispersion characteristics close to the material dispersion of silica due to their small waveguide dispersion resulting from a low index contrast between the core and the cladding.

In contrast, PCFs offer new possibilities for dispersion control due to their tailorable waveguide dispersion. The dispersion profile of PCFs can be tuned by changing the pitch (Λ) and the air-hole size (d). The effect of waveguide dispersion is particularly strong for PCFs with a high air-filling fraction (d/Λ) and small dimensions. By properly choosing the structural parameters, the zero-dispersion wavelength (λ_{ZD}) can be shifted from the near infrared to visible wavelengths [4]. It is also possible to obtain very high dispersion values which are of interest in dispersion compensation [54-56] as well as nearly flat dispersion profiles with low dispersion values [57-59]. Furthermore, for an appropriate choice of the

pitch and air-hole size, PCFs can exhibit two λ_{ZD}s [60]. For illustration, the dispersion profile of a SMF and three PCFs [P2, P4] employed in the thesis are presented in Fig. 4. The profiles of PCFs were calculated using a beam propagation method [61]. The dispersion profile of the 10.8 μm core PCF is close to that of the SMF whereas the 2 μm core PCF exhibits a λ_{ZD} at the visible and near infrared regions due to high waveguide dispersion. Dispersion causes temporal broadening of a pulse traveling along a fiber as the different spectral components of the pulse propagate at different velocities [50].

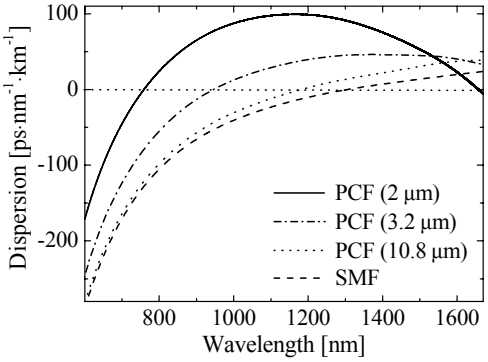

Figure 4. Calculated dispersion profile for a standard SMF, a 2 μm core (Λ=1.4 μm, d/Λ=0.65), a 3.2 μm core (Λ=2.1 μm, d/Λ=0.45) and a 10.8 μm core (Λ=7.1 μm, d/Λ=0.45) PCF.

Birefringence and polarization-mode dispersion

Birefringence in optical fibers results from small variations in the cylindrical symmetry of the fiber and from asymmetrical stress distribution [50, 53]. Due to the local fluctuations in the core shape and stress distribution in the fiber, birefringence changes randomly along the fiber. This phenomenon is commonly referred to as polarization-mode dispersion [50, 53] and can limit the data transmission in long distance high bit-rate communication systems.

The large refractive index contrast of PCFs enables high form birefringence whereas the unique manufacturing process gives a precise control over the cross-sectional index profile. The birefringence in PCFs is usually based on the asymmetrical shape of the core or the cladding microstructure [7, 48] and birefringence of more than an order of magnitude higher compared with conventional optical fibers has been reported [54]. Moreover, the birefringence in PCFs is robust against temperature variations due to the single fabrication material. This unique property can be exploited in, e.g., gyroscopes, interferometers and polarimetric sensors. Furthermore, it is possible to induce stress birefringence in PCFs, which allows for the realization of polarization-maintaining single-mode large-mode area fibers.

Nonlinearity

The manufacturing process of PCFs allows for the fabrication of fibers with a very small core diameter (~1-2 μm) and a high air-filling fraction. Consequently, the propagating modes can exhibit very small effective mode areas compared with conventional fibers [62-64]. As the magnitude of the nonlinear coefficient is inversely proportional to the mode area [31], narrow-core PCFs can exhibit high nonlinearities [63]. The high nonlinearity combined with the special dispersion properties of PCFs provides new possibilities in nonlinear optics. Furthermore, the mode area of PCFs can be wavelength dependent. This can be exploited in the realization of wavelength dependent nonlinear effects [65]. On the other hand, PCFs with a large mode area [18, 66] and, thus, low nonlinearity have also been reported.

3 Polarization properties of microstructured fibers

The polarization characteristics of optical fibers play an important role in, e.g., optical communications and measurement science. In various sensing and device applications, a high degree of birefringence is often desirable whereas in optical communications it is necessary to employ fibers exhibiting low birefringence and polarization-mode dispersion (PMD). While the polarization properties of conventional optical fibers have been studied thoroughly, increasing attention has only recently been turned towards the polarization effects in photonic crystal fibers [7, 48]. Furthermore, the special structure and properties of such fibers may prevent the use of conventional measurement techniques to evaluate the amount of birefringence and PMD [7].

In the first and second section of this Chapter, the polarization properties of optical fibers and the traditional measurement methods commonly employed are shortly discussed. The third section introduces different techniques used to induce birefringence in standard optical fibers and microstructured fibers. Furthermore, the polarization characteristics of narrow-core and polarization-maintaining large-mode area MFs are discussed. The last section of this Chapter deals with the PMD of large-mode area MFs.

3.1 Birefringence and polarization-mode dispersion

Birefringence

In general, optical fibers possess two orthogonal polarization modes [50, 67]. In an ideal optical fiber with a perfectly circular core, these modes are degenerate and their propagation constants are equal. In practice, geometrical asymmetries and non-uniform stress distribution lift the degeneracy. As a result, the polarization modes have different propagation constants and group velocities. In a uniformly birefringent fiber, the polarization modes correspond to the fast and the slow birefringence axes of the fiber. The axis with the larger/lower mode index is called the slow/fast axis. Consequently, the mode with a propagation constant β_s, corresponding to the slow axis of the fiber, possesses a smaller group velocity than the one corresponding to the fast axis (β_f). The modal (phase) birefringence is defined as the difference between the propagation constants or mode indices of the slow and the fast polarization mode [50, 68]

$$\Delta\beta = \beta_s - \beta_f = \frac{\omega\left(n_s - n_f\right)}{c} = \frac{2\pi}{\lambda}\Delta n\,, \tag{1}$$

where ω is the angular frequency of the light, c represents the speed of light in vacuum, Δn is the difference between the mode indices of the orthogonally polarized modes and λ denotes the wavelength of light in vacuum. Other important parameters describing the polarization properties of an optical fiber are beat length, differential group delay and PMD. The beat length (L_b) is the distance over which the two orthogonal polarization modes experience a relative phase change of 2π [50, 69]

$$L_b = 2\pi/\Delta\beta = \lambda/\Delta n\,. \tag{2}$$

The phase delay between the polarization modes ($\Delta\tau_p$) can be presented using the definition of the beat length as

$$\Delta\tau_p = \Delta nL/c = \lambda L/cL_b , \tag{3}$$

where L denotes the fiber length. For a typical SMF with a beat length of 25 m, a value of $\Delta\tau_p$ normalized with a fiber length L is ~0.2 fs/m at 1550 nm.

Differential group delay

The difference between the propagation constants of the polarization modes is associated with a difference in the group velocities ($v_g=(d\beta/d\omega)^{-1}$). As a consequence, the modes split as they propagate through a birefringent section with a length, L. The time separation between the modes ($\Delta\tau_g$) is referred to as differential group delay (DGD) and is defined as [50, 67]

$$\Delta\tau_g = \frac{d(\Delta\beta)}{d\omega}L = \left(\frac{\Delta n}{c} + \frac{\omega}{c}\frac{d\Delta n}{d\omega}\right)L = \left(\frac{\Delta n}{c} - \frac{\lambda}{c}\frac{d\Delta n}{d\lambda}\right)L . \tag{4}$$

Alternatively, DGD can be written in terms of the phase delay as

$$\Delta\tau_g = \left(\Delta\tau_p - \lambda\frac{d\Delta\tau_p}{d\lambda}\right). \tag{5}$$

Figure 5 illustrates the splitting of a pulse in a birefringent fiber when a linear input polarization state is at an angle of 45° to the slow and fast axis. At the input, the electric field of the light resolves into two polarization modes which then separate due to birefringence.

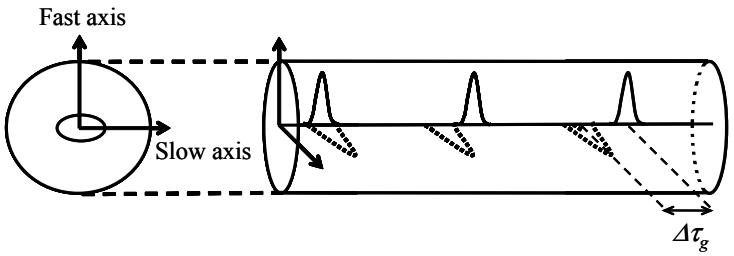

Figure 5. Influence of birefringence on pulse propagation in a polarization-maintaining fiber when both axes are equally excited with a linear input polarization state.

Polarization-mode dispersion

The birefringence in optical fibers changes randomly due to variations in the core size and stress distribution in the fiber. In a long optical fiber, the birefringence is associated with random polarization mode coupling [67-76]. Such a fiber can be represented as a concatenation of random length fiber sections with randomly oriented principal axes of polarization and varying degree of birefringence [53]. Figure 6 presents the principle of polarization mode coupling in the case of two sections A and B. In long fiber spans, coupling is repeated a large number of times along the fiber length. A short light pulse exciting both the fast and slow polarization mode of the section A is coupled to the fiber. After propagating through the first uniformly birefringent fiber segment, the polarization modes are split. At the output of the fiber section, the electric field of the modes is projected onto the polarization modes of the subsequent segment [53]. The local birefringence in the second section then

causes the modes to split apart as can be seen in Fig. 6. As a result of randomly changing birefringence and polarization mode coupling, the light pulse broadens with propagation. This phenomenon is commonly referred to as polarization-mode dispersion (PMD) [67-77]. As differential group delay varies randomly with time, temperature and wavelength, PMD must be treated statistically [53, 70, 74, 77]. Generally, PMD is expressed as either the mean DGD ($\langle \Delta\tau_g \rangle$) or the root-mean-square value of the DGD ($\langle \Delta\tau_g^2 \rangle^{1/2}$) over a particular wavelength range of interest. These are related by [53]

$$\left\langle \Delta\tau_g{}^2 \right\rangle^{1/2} = \sqrt{\frac{3\pi}{8}} \left\langle \Delta\tau_g \right\rangle. \tag{6}$$

In long optical fibers with strong mode coupling, PMD increases with the square root of the fiber length whereas in short fibers it is directly proportional to the fiber length [31, 73]. Polarization-mode dispersion is commonly characterized by a PMD coefficient given in units of ps/km$^{1/2}$.

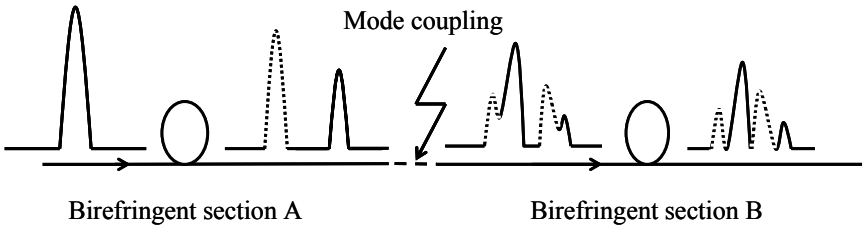

Figure 6. Effect of birefringence and polarization mode coupling to pulse propagation. Dashed line represents the slow polarization mode and the solid line the fast mode of the section A and B.

3.2 Measurement of birefringence and polarization-mode dispersion

Various techniques have been developed to measure birefringence and polarization-mode dispersion in optical fibers. The measurement techniques and devices employed in the thesis (optical frequency-domain reflectometer, Jones Matrix Eigenanalysis, fixed analyzer method, twist method) are shortly introduced in this section [P1, 53]. Furthermore, the effect of a limited measurement bandwidth on the accuracy of PMD measurements is discussed. Special care has to be taken in the selection of the measurement methods as it has been shown that all conventional measurement techniques do not work properly with MFs [7].

Optical frequency domain reflectometer

A polarization-sensitive optical frequency-domain reflectometer (OFDR) is based on a high-resolution coherent reflectometric technique which is used to evaluate the L_b of the fiber [78, 79]. A beat signal between distributed reflections from a fiber under test and a fixed Fresnel reflection from a local oscillator is detected while the frequency of the laser is swept in linear steps. This allows for mapping the measured beat frequencies on a distance scale and, subsequently, determining the fiber reflectivity at a given distance. In a birefringent fiber, the polarization state of the light changes periodically as the light propagates along the fiber. This change translates into oscillations in the detected signal. One oscillation period corresponds to the L_b. When compared with an optical time domain reflectometer, the OFDR provides a higher spatial resolution, sensitivity and dynamic range. The precision of the OFDR measurement is ~1 %/8 % for fibers with low/high polarization mode coupling [79].

Fixed analyzer method

In the fixed analyzer (FA) method, light from a broadband or a tunable narrowband source is coupled into a device under test (DUT) through a polarizer [53]. Subsequently, the output spectrum after the DUT and another polarizer referred to as an analyzer is measured with, e.g., an optical spectrum analyzer. As the polarization states for different wavelengths evolve in different ways along the fiber, the measured transmission spectrum typically exhibits peaks and valleys. The mean DGD can be calculated from the number of extrema within the spectrum when the mode-coupling factor k (k=1 for weak coupling and k=0.824 for strong coupling) is known [53]. The k-factor describes the wavelength dependence of the principal states of polarization. Detection of the output polarization with a polarimeter makes the measurements less sensitive towards the changes of optical power and launch polarization.

Jones matrix eigenanalysis

The Jones Matrix Eigenanalysis (JME) technique [53, 75] typically employs a tunable laser, a polarizer, a polarimeter and a computer to calculate the Jones matrix of the DUT. A polarized signal can be represented as a Jones vector, which describes the amplitude and the polarization state of the signal. The Jones matrix can be obtained from the response of the DUT to three polarization states. It relates the input and output Jones vectors together and characterizes the polarization transforming characteristics of the DUT to within a complex constant that represents the absolute propagation delay. The absolute delay is not involved in the determination of the DGD. The DGD at a certain wavelength can be obtained by solving the eigenvalues of the matrix product given in Ref. 75. The JME technique provides a higher accuracy and dynamic range (~1 fs-1000 ps) compared with the FA method (~0.05-400 ps).

Twist method

The twist method [80, 81] utilizes the JME technique to measure DGDs at the different twist rates of the fiber and, as a result, provides both the phase and group birefringence for an untwisted fiber. Twisting the fiber induces circular birefringence and mode coupling between the polarization modes. For low twist rates, the coupling leads to a drop in the DGD, whereas the DGD starts to increase again for large twist rates as the additional circular birefringence becomes dominant. For this method to be practical, the L_b should be within ~5 mm to 1 m.

Measurement limitation of polarization-mode dispersion

The intrinsic PMD measurement limitation stems from the fact that the DGD is a statistical quantity due to random mode coupling and variations in local birefringence. The value of the DGD is wavelength sensitive and DGD at one wavelength changes over time due to varying environmental conditions. A finite measurement bandwidth imposes a limitation on the accuracy of the PMD measurements. The measurement limitation common for all the measurement methods that average DGD over a wavelength range can be expressed as [74]

$$PMD_{meas} = PMD_{theo} \cdot (1 \pm \frac{0.9}{\sqrt{PMD_{theo} \cdot \Delta\omega}}), \quad (7)$$

where PMD_{meas} denotes the measured PMD value, PMD_{theo} is the theoretical mean PMD and $\Delta\omega$ the measurement bandwidth. Consequently, for a small PMD value, the employed measurement range needs to be sufficiently broad in order to determine the PMD precisely. The accuracy of modern commercial measurement instruments is close to the abovementioned theoretical limitation.

3.3 Birefringent microstructured fibers

The hexagonal cladding structure of MFs should not allow for inherent birefringence due to symmetry constraints [82]. In practice, as is the case with conventional optical fibers, the fiber structure is always to some degree asymmetric leading to local birefringence. Moreover, the flexibility in the design of MFs offers the possibility of manufacturing structures that exhibit high degree of birefringence. In this section, the methods utilized to induce birefringence in optical fibers are briefly introduced. Subsequently, the polarization properties of narrow-core and stress-birefringent MFs are discussed. It is shown that the birefringence characteristics of these fiber types can be qualitatively different in comparison with conventional optical fibers and, consequently, special attention is required when predicting the polarization properties of MFs.

Polarization-maintaining conventional and microstructured fibers

Several techniques can be applied to induce form and stress birefringence in optical fibers [31, 50]. The most commonly used methods are either based on an elliptical core design or on stress applying parts positioned in the cladding close to the fiber core [83-85]. In the first case, the degree of birefringence depends on the square of the refractive index difference between the core and cladding and on the core size and ellipticity [86] whereas in the latter case it depends on the stress-optic coefficient of the fiber material and on the position, shape, size and material of the stress elements [84, 85]. In Fig. 7, schematic pictures of a) form- and b, c) stress-birefringent fibers are illustrated. In general, conventional polarization-maintaining fibers exhibit phase birefringence (Δn) on the order of ~ 10^{-4} [50]. Such fibers are commonly used in applications requiring light to preserve a linear polarization state.

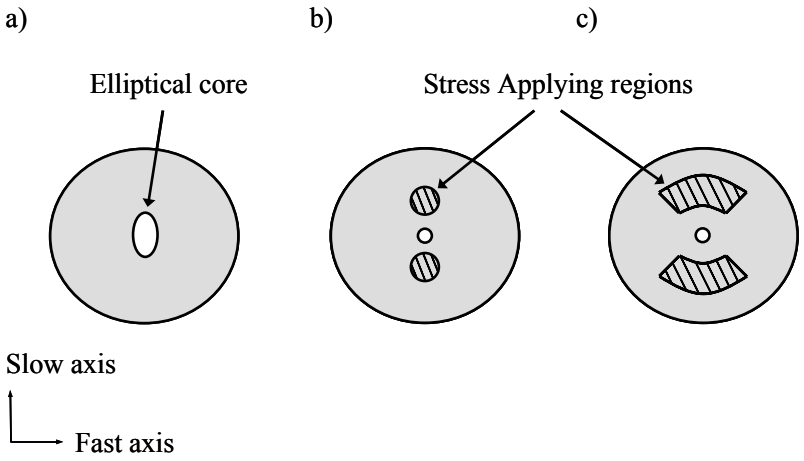

Figure 7. Polarization-maintaining optical fibers: a) elliptical core, b) Panda and c) Bow-tie fiber.

The stack-and-draw method and the high refractive index contrast between silica and air allow for the fabrication of highly birefringent MFs [7, 48, 54, 87]. To date, the highest reported values for phase and group birefringence are $4.5 \cdot 10^{-3}$ and $7.5 \cdot 10^{-3}$, respectively [54]. Different MF designs with elliptical cladding holes [88], an asymmetrical core [48, 89], different sized cladding holes adjacent to the core [7, 87, 90] and hybrid material MFs with tunable birefringence [91] have been proposed and demonstrated. While these fibers exhibit high birefringence, they also possess a relatively small core size that causes a power

limitation and makes the use of the fibers difficult. A combination of a large-mode area and a relatively high birefringence ($\Delta n \approx 10^{-4}$) can be obtained by employing MFs with stress applying elements [92, P1]. Such a fiber can also provide single-mode operation over a wide wavelength range. In addition, PCFs that guide only one polarization mode of a light signal have been realized [93]. Moreover, the birefringence in single-material MFs is resilient towards temperature changes making them good candidates for sensing applications [P1, 94]. Optical microscope images of a stress-birefringent and an elliptical core MF are shown in Fig. 8. The polarization properties of PBFs [96] are beyond the scope of this thesis and only the properties of index-guiding MFs will be discussed in the following.

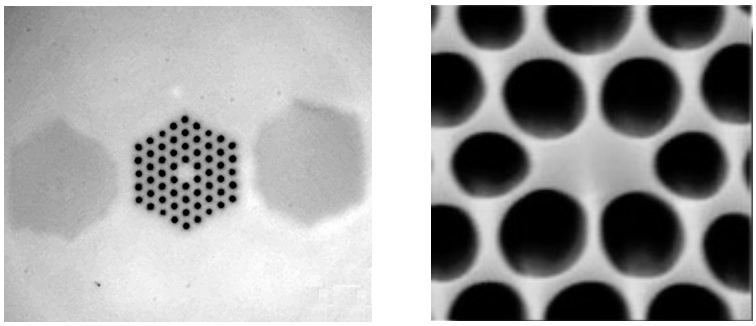

Figure 8. Cross-section of a MF with stress applying parts (left) [P1] and an elliptical narrow-core MF (right) [95]. In both cases the slow axis is oriented horizontally.

Group and phase birefringence in microstructured fibers

In the presence of strong form birefringence, differential group and phase delays have typically different values although at a specific wavelength they can be of the equal magnitude [81]. On the other hand, in the presence of large stress-induced birefringence, the differential group and phase delays are of the same magnitude and their ratio is nearly constant with wavelength [81]. Consequently, the ratio of group and phase birefringence can indicate whether the birefringence is due to form or stress contributions. In particular, MFs are known to exhibit accidental form birefringence and strongly wavelength dependent optical characteristics and, therefore, the usual assumption of equal group and phase birefringence in optical fibers may not always be true for MFs. To date, only a few experimental studies of the polarization properties of MFs including results on both the differential group and phase delay have been reported [e.g. 81, 97, 98]. As is shown later in Section 3.4, it is possible to manufacture LMA-MFs with low birefringence and PMD [P2]. However, it is more complicated to obtain low birefringence in narrow-core MFs as they easily suffer from rather strong unintentional form birefringence. This arises as a result of accidental geometrical imperfections occurring during the fiber fabrication.

In Paper P1, the phase and group birefringence of narrow-core MFs with unintentional birefringence and PANDA MFs were investigated and compared with that of a standard PANDA fiber. The same type of boron-doped silica stress elements were used in all PANDA fibers. Also, the robustness of birefringence to changes in environmental conditions was studied. The differential phase delay ($\Delta\tau_p$) and group delay ($\Delta\tau_g$) of Eqs. (3) and (4) normalized with the fiber length were used to evaluate the corresponding type of birefringence. Table 2 summarizes the characteristics of the fiber samples and gives the corresponding ratios of differential group to phase delay at a wavelength of 1550 nm.

Table 2. Characteristics and ratio of normalized differential group to phase delay @ 1550 nm for narrow-core and PANDA MFs. *d*: air-hole diameter and *Λ*: pitch.

	MF-1	MF-2	PANDA-1	PANDA-2	PANDA-3	Standard PANDA
Core size [μm]	2	3.5	4.9	7	9.1	10.5
***Λ* [μm]**	1.4	2.3	3.2	4.4	5.9	
d/Λ	0.6	0.4	0.48	0.48	0.48	
$\Delta\tau_{g,\,n} / \Delta\tau_{p,\,n}$	0.38	1.27	1.61	1.30	1.09	1.1

All the studied MFs were found to exhibit strong phase and group birefringence although their birefringence was lower compared with a standard PANDA fiber [P1]. In most cases, the ratio of differential group to phase delay differs from one indicating the presence of form birefringence [81]. A ratio close to one was only found for the standard PANDA fiber and the largest PANDA MF suggesting that the contribution of form birefringence is very small in these fibers. This is consistent with the fact that the influence of accidental form birefringence decreases with increasing core size [99]. As a matter of fact, one observes a monotonic decrease in the ratio of differential group to phase delay with increasing core size for PANDA MFs. The results illustrate the difficulty in fabricating narrow core MFs with a low accidental form birefringence and that the commonly used assumption of equal group and phase birefringence does not always hold in the case of MFs. Consequently, special care has to be taken when predicting the birefringence characteristics of MFs.

Wavelength dependence of polarization characteristics

In order to investigate the presence of form birefringence in more detail, the wavelength dependence of birefringence was studied in Paper P1. The differential phase delay of narrow-core MFs was observed to increase nearly linearly with wavelength, which agrees with other experimental and numerical results [e. g. 97, 99-103]. However, the wavelength dependence of the DGD was different for the narrow-core MFs. For the 2 micron core MF, the DGD decreased with wavelength whereas for the 3.5 micron core MF it increased with wavelength indicating that the delays strongly depend on the fiber geometry. For the largest PANDA MF, the wavelength dependence of the differential group and phase delays was small and the delays were of equal magnitude. In contrast, for the smallest PANDA MF, the DGD was observed to increase with wavelength and its magnitude was different from the value of the differential phase delay.

The ratio $\Delta\tau_{g,\,n}/\Delta\tau_{p,\,n}$ is plotted in Fig. 9 as a function of wavelength for two narrow-core and PANDA MFs. In the case of the narrow-core MFs and the smallest PANDA MF, the ratio differs from one and changes significantly with wavelength indicating the presence of form birefringence. The ratio is close to one and nearly constant with wavelength only for the largest PANDA MF. As a consequence, such a fiber seems to be more suitable for applications requiring a small wavelength dependence of birefringence. The results indicate that the largest PANDA MF exhibits similar polarization properties as a standard PANDA fiber while it is expected that the smallest PANDA MF is subject to some amount of form birefringence and, thus, its polarization characteristics are somewhere between the narrow-core MFs and standard PANDA fibers.

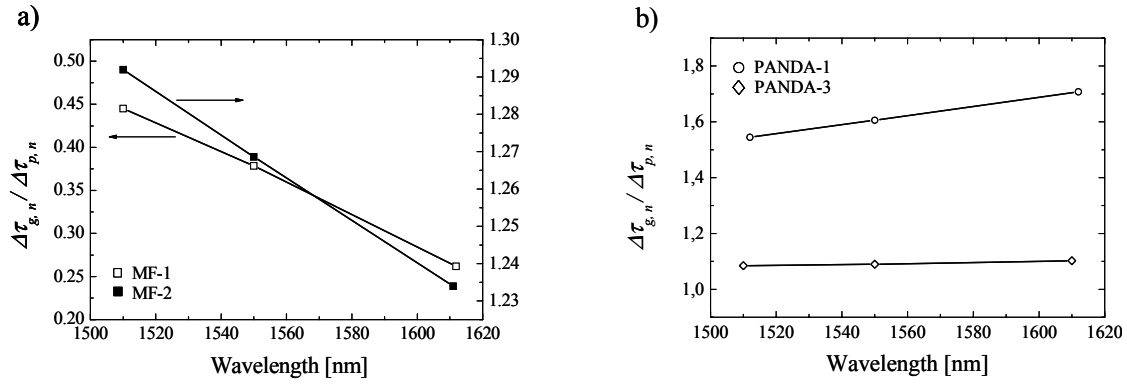

Figure 9. Ratio of normalized differential group to phase delay as a function of wavelength for a) narrow-core and b) PANDA MFs.

Temperature dependence of polarization characteristics

In polarization-maintaining applications and polarimetric fiber sensors, it is important to take into account the sensitivity of the polarization properties to changes in environmental conditions. In particular, temperature fluctuations can affect the stability of many fiber-based systems. In contrast to conventional optical fibers, MFs fabricated from a single material do not suffer from a temperature sensitive internal birefringence resulting from the different chemical compositions of the core and the cladding. The small temperature dependence of the birefringence results mainly from a change in the effective refractive index difference between the core and the cladding [101, 102]. The refractive index of the core grows more rapidly with temperature than the effective index of the cladding that is influenced by the refractive index of air. In the case of PANDA fibers, birefringence is introduced by placing two boron-doped silica stress parts, with a larger thermal expansion coefficient than that of silica, outside the holey cladding. The birefringence arises from a stress field which is induced while the fiber is cooled during the fabrication. These fibers are, therefore, more sensitive to temperature variations.

The dependence of the phase birefringence on the temperature can be quantified through the parameter $K_T = \partial(\Delta\beta)/\partial T$ whereas the temperature dependence of the group birefringence can be characterized by $K_\tau = \partial(\Delta\tau_g)/\partial T$ [P1]. The values of K_T and K_τ normalized with $\Delta\beta$ (phase birefringence in radians) and $\Delta\tau_g$ can be used as the figures of merit for the temperature dependence of the phase and group birefringence, a smaller value corresponding to a less temperature sensitive birefringence. The normalized values of K_T and K_τ for a narrow-core MF and different PANDA fibers are presented in Table 3.

Table 3. Normalized temperature sensitivities of phase birefringence ($\Delta\beta$) and differential group delay ($\Delta\tau_g$) @ 1550 nm.

	MF-1	PANDA-1	PANDA-3	Standard PANDA
$K_T/\Delta\beta$ [1/K]	$1.66\cdot10^{-5}$	$-1.65\cdot10^{-3}$	$-1.38\cdot10^{-3}$	$-1.37\cdot10^{-3}$
$K_\tau/\Delta\tau_g$ [1/K]	$1.2\cdot10^{-4}$	$-1.47\cdot10^{-3}$	$-1.44\cdot10^{-3}$	$-1.3\cdot10^{-3}$

Compared with the PANDA fibers, the relative temperature sensitivities of the phase and group birefringence for the narrow-core fiber are smaller by a factor of 100 and 10, respectively. Furthermore, the relative change of the differential group delay with temperature is roughly seven times larger than that of the differential phase delay in the narrow-core fiber. The normalized K_T values are almost identical for the three PANDA fibers. This can be explained by the fact that the same type of stress elements are used in all these fibers leading to an equal change of stress with temperature. Although the birefringence resulting from the asymmetric stress field differs among the fibers, its relative change with temperature remains the same. Also, the normalized K_τ values for the PANDA fibers are of the same magnitude. The results show that narrow-core MFs are promising candidates for temperature insensitive sensor and interferometer applications [101, 104, 105] whereas single-mode LMA PANDA MFs could be useful in polarization-maintaining high-power applications which do not possess so strict temperature requirements [106].

3.4 Polarization-mode dispersion of large-mode area microstructured fibers

Improvements in manufacturing technology have allowed for the fabrication of long MFs with a uniform structure and low loss at the optical telecommunications window [10, 49]. This progress has made MFs attractive candidates also for optical communications. In particular, the possibility of fabricating endlessly single-mode LMA-MFs is interesting from many aspects [5, 18, 107, 108]. For example, the large core area reduces the risk of material damage and the impairments arising from various nonlinear effects [16]. Larger dimensions allow also for a better control of the microstructure during the manufacturing process and reduce the possibility of accidental birefringence which is likely to occur for smaller size of the structure. In long optical fibers, local birefringence is combined with random polarization mode coupling leading to PMD. In particular, fibers exhibiting low birefringence and PMD are required in high bit-rate communication systems operating over long distances.

In Paper P2, the PMD and birefringence of LMA-MFs were studied using the measurement techniques described in Section 3.2 [53, 68]. Table 4 shows the fiber characteristics. The ratio of the hole diameter, d, to the pitch of the structure, Λ, is in the range of 0.45-0.50 for all the fibers, which ensures single-mode guidance from visible to infrared wavelengths [108]. The intensity profiles of the fundamental mode propagating in LMA-MFs simulated using a beam propagation method (BPM) [61] are shown in Fig. 10 for a wavelength of 1500 nm. The simulations show that the fundamental mode is well confined within the core for all the fibers. Therefore, it is expected that the symmetry of the innermost cladding-hole ring has the greatest impact on birefringence.

Table 4. Properties of LMA-MFs @ 1550 nm. Λ: pitch, L_b: beat length, λ_{ZD}: zero-dispersion wavelength.

	LMA-1	LMA-2	LMA-3
Core size [μm]	10.8	14.8	19.4
Λ [μm]	7.1	9.7	12.7
Length [m]	102	101	101
L_b [m]	0.73	21	1.6
λ_{ZD} [nm]	~1175	~1215	~1230

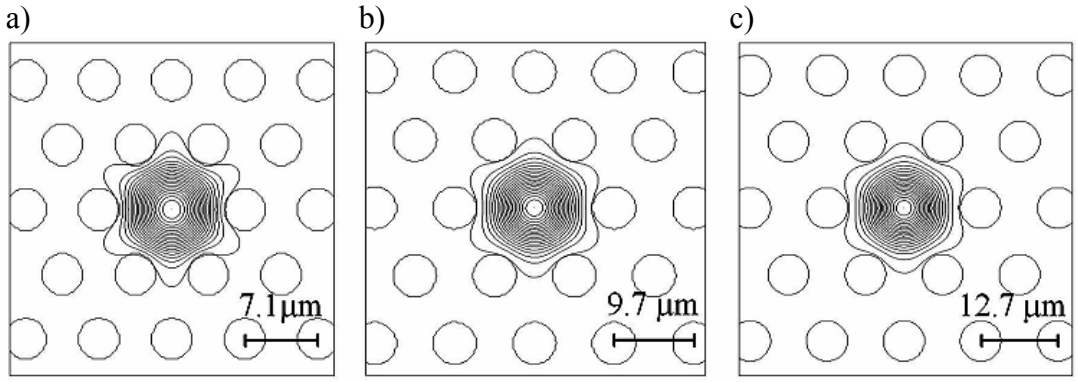

Figure 10. a) Contour plots of the fundamental mode propagating in a) LMA-1, b) LMA-2 and c) LMA-3 at 1500 nm simulated using the BPM method. Contour lines are spaced by 0.05 dB.

Figure 11 displays several DGD measurements for the 10 micron core MF performed using the JME method. The measurements show that there are only small variations from one measurement to another while the external conditions are kept unchanged (ΔT= 2 °C). All the

traces exhibit strong variations of DGD with wavelength, which is a clear indication of strong polarization-mode coupling. This was further confirmed by the PMD values obtained with the FA method, which agreed better with the JME results when assuming strong polarization mode coupling (k=0.824) [P2]. The measurements conducted with the 15 and 20 micron core fibers showed also variations of DGD with wavelength suggesting that such fibers are prone to mode coupling.

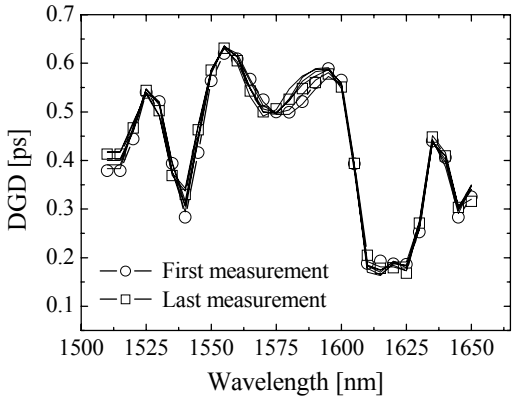

Figure 11. Series of eight DGD measurements performed over a test period of 19 days for a 10 µm core MF. PMD values of the measurements vary between 0.427-0.435 ps.

Although fairly large mode coupling was observed for all the fibers, the 15 micron core fiber was found to exhibit low local birefringence [P2]. The beat length (L_b) of the fiber was 21 m (1550 nm) and varied only slightly with distance. The long beat length results in birefringence (Δn) of ~$7.4 \cdot 10^{-8}$. Both the L_b and Δn are close to the values reported for SMFs ($L_b \approx$20-30 m, $\Delta n \approx 10^{-7}$) [50, 81]. Also, the PMD coefficient of the fiber (~0.02 ps/km$^{1/2}$) was comparable to the ones of the state-of-the-art SMFs (~0.05 ps/km$^{1/2}$ [31]). A microscope image of the 15 micron core fiber is presented in Fig. 12. The image shows a high degree of symmetry in the hole structure, which is typical for fibers with low form birefringence.

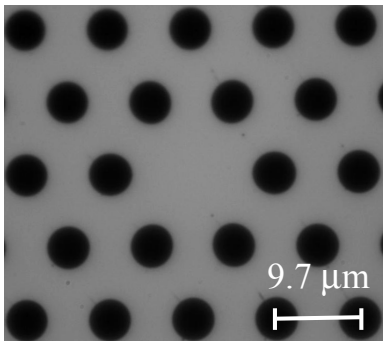

Figure 12. Optical microscope image of the core and the nearest cladding rings of the 15 µm core MF.

In order to assess the reliability of the PMD measurement techniques applied to MFs, PMD measurements of LMA-MFs were conducted at three different places (Helsinki University of Technology, University of Geneva and Crystal Fibre A/S). As could be expected for the fibers exhibiting strong polarization mode coupling, the measurements performed at the same place agreed well together whereas the agreement was somewhat worse for the measurements conducted at different facilities. Nevertheless, the PMD values were still within the intrinsic measurement limitation [P2, 74]. The consistency of the results suggests that the employed measurement techniques work reliably. The lowest measured PMD values were in the order of 5-10 fs for a 100 m long 15 micron core MF whereas the other 100 m

long samples exhibited PMD values in the range of 150-450 fs. The low birefringence and PMD of the 15 micron core MF indicate an excellent symmetry in the fiber structure over a long length. Therefore, it is expected that LMA-MFs could find use also in optical communication applications. Besides manufacturing fibers with a high structural symmetry and, consequently, low form birefringence, PMD can be reduced by introducing spin into the fiber during the draw. This increases light coupling between the polarization modes and, thereby, levels off the propagation times of the modes. The effect of spin on PMD is not studied in this thesis, however, it has been later demonstrated that spinning can be exploited to further reduce PMD in LMA-MFs [109].

Temperature dependence of polarization-mode dispersion

As mentioned earlier, the total birefringence in an optical fiber is a combination of a geometrical (form) and stress-induced birefringence [50]. In addition, the stress birefringence can be sensitive to the temperature. Although MFs are made from a single material having a uniform composition, coating material can induce stress in optical fibers [110] and change the PMD characteristics. The coating of the LMA-MFs is a single-layer acrylate coating, in contrast to conventional dual-layer coatings with a soft buffer layer between the glass cladding and acrylate [P2]. Hence, the glass of the fiber is in direct contact with the coating material and, therefore, poorly shielded from externally applied pressure and stresses in the coating. As the coating has a much higher thermal expansion coefficient [P2] than silica, the stress caused by the thermal contraction mismatch between silica and coating material may induce birefringence and change the polarization mode coupling.

In Paper P2, the effect of temperature on the PMD characteristics of single-coated LMA-MFs was studied. The experimental setup and a typical temperature dependence of the PMD for the 10 micron core MF are shown in Fig. 13. The variation of the PMD with temperature occurs in two distinct stages. First, the PMD decreases while the temperature rises until the temperature reaches ~40 °C. For higher temperature values, the PMD stays almost constant. The results obtained with both the FA and JME methods confirmed this behavior. Similar results were also obtained with the 20 micron core MF. However, the PMD of the 15 micron core MF was too low to allow for accurate measurements. These results indicate that the coating induces thermal stress on the fiber at low temperatures whereas increasing the temperature above ~40 °C eliminates partly the external contributions to the total stress. The results presented in Paper P2 indicate the possibility of fabricating LMA-MFs exhibiting, to a large extent, temperature insensitive PMD by employing more advanced coating structures.

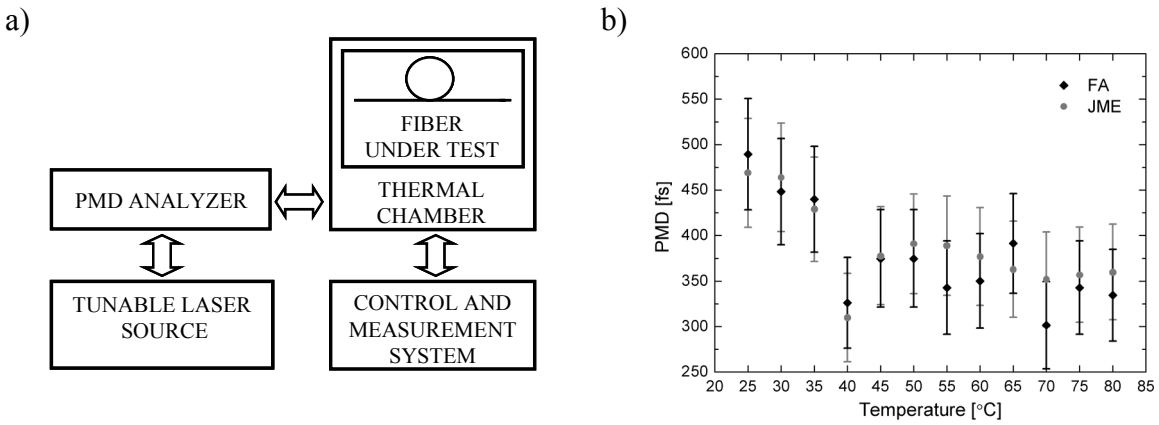

Figure 13. a) Experimental setup for measuring the temperature dependence of the PMD. b) Temperature dependence of the PMD for a 10 µm core MF (k=0.824 for FA method).

4 Supercontinuum generation using nanosecond pulses

The propagation of high power light pulses in a nonlinear medium can lead to substantial spectral broadening of the input pulse bandwidth. The broad spectrum resulting from cascaded nonlinear processes is often referred to as supercontinuum (SC) [111]. Supercontinuum was first demonstrated in a borosilicate glass sample in 1970 [112]. This was followed by SC generation in liquids [113], gases [114] and in optical fibers [115, 116]. An important step towards ultra broadband SC generation was taken by the introduction of MFs. Microstructured fibers can exhibit special dispersion characteristics and strong field confinement which results in enhanced nonlinear properties that allow for improving the spectral bandwidth of the SC [8, 117, 118]. The first SC in a highly nonlinear MF was demonstrated in 1999 [8, 119]. Large-bandwidth continua have also been generated by employing tapered fibers which possess a reduced effective area and, therefore, enhanced nonlinearity [120]. Supercontinuum sources find applications in various areas including optical frequency metrology [17, 121], coherent optical tomography [21, 22], optical component characterization [19, 20, 122] and optical communications [23].

The first section of this Chapter briefly introduces the nonlinear mechanisms involved in the SC generation using nanosecond pulses. In the second and third sections, the SC formation in LMA-MFs [P3] and narrow-core MFs is discussed. Supercontinuum generated in narrow-core MFs is applied in Section 5.3 where the combination of a broadband light source and a gas cell in a single MF is demonstrated [P4].

4.1 Physics of supercontinuum generation using nanosecond pulses

In the following, the physical mechanisms responsible for SC generation using ns pump pulses are shortly discussed. Since the peak power of these pulses is usually lower than in the case of fs pulses, several meters of fiber are typically needed to generate the SC [123-125]. Also, the influence of self-phase modulation in the SC generation is negligible as the temporal pulse width is broad [31]. The mechanisms involved in the SC formation depend on whether the pump wavelength (λ_p) is located in the normal or anomalous dispersion region of the fiber. The two cases are reviewed below.

Pump wavelength in normal dispersion

When the pump wavelength is located in the normal dispersion region, the formation of the SC is initiated by cascaded stimulated Raman scattering (SRS) [31, 126]. In SRS, energy is transferred from a pump wave to a Stokes wave at a longer wavelength. If only the pump wave is traveling along the fiber, quantum noise sources (shot noise and spontaneous Raman scattering) act as a probe and are, subsequently, amplified with propagation. Energy can also be transferred to anti-Stokes waves (lower wavelengths) but the process is less efficient in this case [31]

$$2\omega_p \rightarrow \omega_{as} + \omega_{st}\,, \tag{8}$$

where ω_p is the angular frequency of the pump photon and ω_{as} and ω_{st} represent the angular frequencies of the anti-Stokes and Stokes photons, respectively. Stimulated Raman scattering is a broadband effect and can influence signals as far as 40 THz away from the pump. The peak of the gain is located 13.2 THz from the pump [127]. When the pump power exceeds

the Raman threshold [31], the frequency component determined by the maximum gain builds up rapidly. In a similar way, this Stokes wave can act as a pump wave to generate a second-order Stokes wave and so forth, resulting in the generation of multiple Raman lines that are separated by 13.2 THz and extend towards longer wavelengths [31]. An example of this process is illustrated in Fig. 14 where ns pulses at 1064 nm were launched into the normal dispersion region of a LMA-MF.

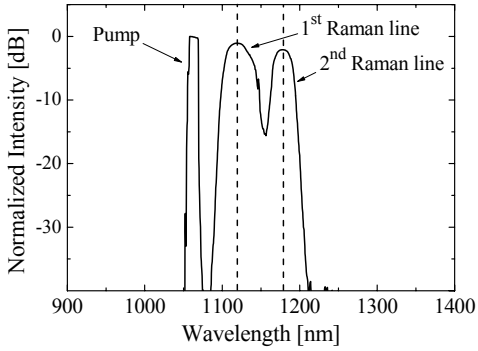

Figure 14. First two Raman lines generated in a 20 μm core MF measured with an optical spectrum analyzer by employing a nanosecond Nd:YAG laser as the pump source. Location of lines agrees well with the 13.2 THz frequency shift induced by Raman scattering.

If the pump power is high enough so that the Raman lines with lower frequencies fall into the anomalous dispersion region of the fiber, these lines can efficiently seed degenerate four-wave mixing (FWM) processes [125, 127, 128] and, thereby, transfer a substantial amount of energy to the anomalous dispersion region. Stimulated Raman scattering and FWM modulate the temporal envelope of the initial pump pulse and break the pulse into multiple subpulses [128, 129]. The subpulses corresponding to the frequency components transferred to the anomalous dispersion region subsequently undergo soliton dynamics. More specifically, these dynamics include the soliton self-frequency shift (SSFS) [130] and the generation of dispersive waves (DWs) [131]. The SSFS arises from the fact that the spectral bandwidth of the sub-pulses can exceed several THz and, therefore, overlap with the Raman gain. Stimulated Raman scattering then constantly transfers energy from the high-frequency to the low-frequency side of these sub-pulse spectra. Consequently, the center frequencies of the sub-pulse spectra experience shift towards the infrared wavelengths with propagation, which leads to a smooth continuum for wavelengths above the zero-dispersion wavelength [127-129]. Furthermore, when the zero-dispersion wavelength is located in the vicinity of the pump wavelength, non-phase-matched FWM can also occur within the normal dispersion regime of the fiber, which initiates broadening of the SC towards blue wavelengths [125, 132, 133]. Also, cross-phase modulation (XPM) between the solitons experiencing the SSFS and the frequency components located in the normal dispersion region extend the SC further to the blue wavelengths [134, P3].

Pump wavelength in anomalous dispersion

When the pump wavelength resides in the anomalous dispersion region, the SC formation is initiated by modulation instability (MI) [125, 128, 129] which refers to the exponential amplification of small perturbations to the steady state. As a result of modulation instability, a fast modulation develops on the top of the temporal envelope of the input pulse. The modulation instability phenomenon is equivalently described in the frequency domain by the degenerate FWM theory of continuous wave fields. In degenerate FWM, two pump

photons (ω_p) are annihilated and two new photons, a Stokes and an anti-Stokes photon, are generated at the frequencies of ω_{st} and ω_{as} [31]

$$2\omega_p = \omega_{as} + \omega_{st}. \tag{9}$$

As every wave mixing process, FWM is strongly dependent on the relative phase of the mixing components. The phase matching condition for this process to be efficient is [31]

$$2\beta_p = \beta_{as} + \beta_{st} + 2\gamma P_p\,, \tag{10}$$

where β_j are the propagation constants of the pump, anti-Stokes and Stokes waves. The frequency shift between the pump and the sidebands, Ω_s, can be obtained from Eqs. (9) and (10) by expanding $\beta_{as}(\omega)$ and $\beta_{st}(\omega)$ in a Taylor series about the pump frequency while retaining up to terms that are quadratic in Ω_s [31]

$$\Omega_s = \omega_p - \omega_{st} = \omega_{as} - \omega_p = \sqrt{\frac{2\gamma P_p}{|\beta_2|}}\,, \tag{11}$$

where γ is the nonlinear coefficient of the fiber, P_p is the peak power of the pump pulse and β_2 represents the group velocity dispersion coefficient at the pump frequency ω_p. The aforementioned condition is readily fulfilled in the anomalous dispersion region of fibers and results in the growth of sidebands symmetrically located around the pump wavelength. As in the case of SRS, noise serves as seed for MI/FWM processes. When the strength of the modulation is large, or equivalently when the spectral sidebands have been substantially amplified, the broad input pulse breaks into multiple extremely short sub-pulses which experience soliton dynamics (SSFS, DWs, XPM) [130, 131, 134]. If the λ_p is substantially detuned from λ_{ZD}, the DWs and XPM are absent and the expansion of the continuum spectrum occurs solely towards infrared wavelengths.

4.2 Supercontinuum generation in large mode-area microstructured fibers

Supercontinua have been typically generated in tens of centimeters-long narrow-core MFs by employing femtosecond laser pulses [8] and in several meter-long narrow-core MFs using picosecond or nanosecond pulses [124, 125]. The power limitation encountered in narrow-core MFs results from the strong field confinement which leads to a high local intensity that can damage the fiber [66]. As an example, the damage threshold of silica is 500W/μm^2 for a pulse width of one nanosecond [135]. Consequently, the threshold is exceeded with less than 2 kW of peak power in the case of a typical narrow-core MF with a 2 micron core diameter [66]. The small core size of narrow-core MFs results also in a large attenuation at the wavelengths of the order of and larger than the core dimension [136]. This can limit the maximum output power and infrared bandwidth obtainable. Furthermore, narrow-core MFs possess a high numerical aperture that leads to a large output beam divergence and, thus, additional optics is required to couple light into optical components. These fibers can also suffer from multi-mode operation and high birefringence [99] that can decrease the efficiency of SC generation. One way to overcome these problems is to employ LMA-MFs in SC generation. Even though their nonlinearity is much lower compared with narrow-core MFs, LMA-MFs typically exhibit lower OH-losses [66, 125, 137] and, thus, allow for the use of longer fiber lengths to compensate for the low nonlinearity. Moreover, LMA-MFs can combine a large core and a low numerical aperture with an endlessly single-mode operation [18, 25]. Large dimensions are easier to control during the fabrication resulting in highly symmetrical structures and, thereby, in low form birefringence and polarization dependence

of the generated SC [P2, 95]. In addition, the relatively large core-size of LMA-MFs facilitates practical handling of fibers. Consequently, LMA fibers can be directly connectorized and spliced to standard SMFs.

Supercontinuum generation in LMA-MFs using ns pump pulses was studied in Paper P3. The light source employed in the experiments was a compact, passively Q-switched Nd:YAG laser operating at 1064 nm [123]. Consequently, the λ_p is located in the normal dispersion region of the LMA-MFs employed (see Table 4) and the mechanism leading to the SC formation is similar to that described in the beginning of the previous section. Typical SC spectra generated in LMA-MFs are shown in Fig. 15. By launching pulses with a higher peak power (2.7 ns pulse width, 5 kHz repetition rate, ~20 mW average coupled power), the bandwidth of the SC is substantially increased for a 15 and 20 micron core fiber compared with the results presented in Paper P3 [66]. For the 20 micron LMA-MF, macrobending losses were observed to limit the SC bandwidth on the short wavelength side [25]. This is in contrast to conventional optical fibers which exhibit macrobending loss at long wavelengths. However, conventional fibers are multi-mode at short wavelengths, which is not desirable in SC generation. When the 20 micron core fiber was wound on a spool with a 16 cm radius, the continuum extended from 700 nm to beyond 1750 nm (-20 dB bandwidth), the optical spectrum analyzer (OSA) limiting the measurable wavelength range. Except for the remains of the pump at 1064 nm, the amplitude variations in the spectrum do not exceed 3 dB over a 700 nm range (920 to 1670 nm). The magnitude of the water peak at 1390 nm for a 90 m long fiber was only ~1 dB which is a clear advantage over narrow-core fibers that typically exhibit much higher OH-losses (see Fig. 16). To illustrate the advantage of the LMA-MFs in high-energy SC generation, the abovementioned experiment was performed with a 2 micron core MF. The tip of the fiber was damaged as the pulse energy was too high indicating that high-energy SC may be difficult to obtain with narrow-core MFs [66]. Large mode-area MF supercontinuum sources may find use in applications requiring high-power single-mode broadband sources with low polarization dependence and low output beam divergence.

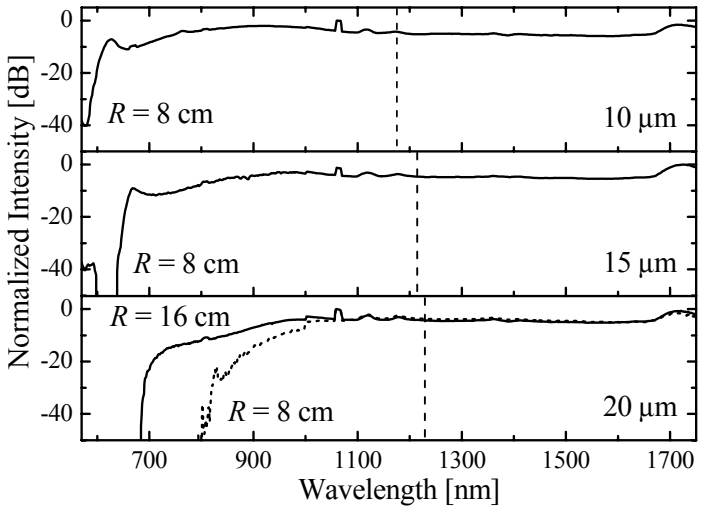

Figure 15. Supercontinuum generated in MFs with a 10, 15 and 20 μm core diameter measured with an optical spectrum analyzer by employing a Nd:YAG laser as the light source. Effect of bending radius R is shown for the 20 μm core fiber. The dashed lines show the location of the λ_{ZD}s.

4.3 Supercontinuum generation in narrow-core microstructured fibers

In the case of narrow-core MFs studied in Paper P4, λ_p was located in the anomalous dispersion region of the fiber. A typical SC generated in a 15 m long 2 μm core MF is shown in Fig. 16 (~3 ns pulse width, 30 kHz repetition rate, ~30 mW average power coupled). The peak at ~1390 nm is due to OH-absorption. The scenario was confirmed through simulations which are plotted in Fig. 17 with the same resolution used in the experiment. For computation time considerations, the initial pulse width was chosen to be 1 ns and the fiber length 10 m. An extended nonlinear Schrödinger equation including the full propagation constant and the delayed Raman response of the fiber as well as the self-steepening effect was used to model the pulse propagation along the fiber [P4, 138]. The simulation reproduces qualitatively the features seen in the experimental spectrum and also shows the generation of short sub-pulses [P4]. The main consequence in neglecting the fiber losses is the absence of the water peak.

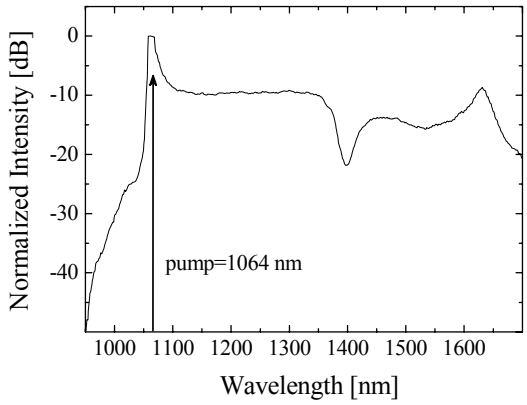

Figure 16. Supercontinuum generated in a 2 μm core MF with λ_{ZD}s at ~750 and 1670 nm (resolution 10 nm).

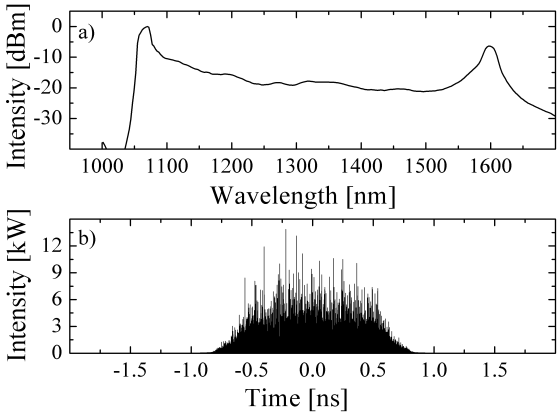

Figure 17. a) Numerical simulation of SC generated in a 10 m long 2 μm core MF for an initial pulse width of 1 ns. b) Simulation of the time trace of the SC.

5 Gas spectroscopy using photonic crystal fibers

The photonic crystal fiber technology has opened up new opportunities in the field of sensing. In particular, the possibility of infiltrating gases or liquids into the holes of PCFs has attracted increasing attention [11-15]. Photonic crystal fibers filled with fluids can offer simultaneously strong light confinement and very long optical interaction lengths in compact fashion. The interaction between light and the gas sample can be exploited in two different ways depending on the fiber type employed. In index-guiding fibers, the evanescent field of the light interacts with the gas present in the holes [12] whereas in air-guiding PBFs ~98% of the mode energy can propagate in a gas-filled hollow core [35].

This Chapter deals with gas spectroscopy using PCFs. In the first and second section of this Chapter, the basics of the absorption spectroscopy and the vacuum system employed in the experiments are briefly discussed. The combination of a broadband light source and a gas cell in a single narrow-core MF is presented in the third section. Section 5.4 focuses on the use of PBFs in gas detection. The last section of this Chapter introduces an optical wavelength reference based on a gas-filled PBF.

5.1 Introduction to absorption spectroscopy

When a light beam is propagating in gas, the energy of the photons can excite molecules to higher energy levels. Each level is quantized and consists of a combination of vibrational, rotational and spin energy levels. Consequently, molecules can only absorb discrete amounts of energy resulting in the loss of light at specific absorption wavelengths. Each molecular species has a unique absorption spectrum from which they can be identified. A typical absorption spectrum consists of absorption bands that again comprise a number of closely spaced absorption lines. The wavelength ranges of the absorption spectra of various molecules in the near infrared region are presented in Fig. 18 [139-141]. The figure also marks the locations of optical telecommunication bands which are discussed later in the Section 5.5. Generally, in absorption spectroscopy, light transmission through a sample is measured as a function of frequency or wavelength. This can be done by utilizing a monochromatic tunable light source and a detector or a broadband source such as a light emitting diode (LED) and an OSA. Information about the molecule concentration or the molecular content of the gas is, subsequently, retrieved from the measured absorption. According to the Beer-Lambert law, the transmitted (I_T) and incident power (I_0) are related by [142]

$$I_T = I_0 \cdot e^{-\alpha \cdot L_p}, \tag{12}$$

where L_p represents the path length, and α denotes the absorption coefficient. More specifically, the absorption coefficient at frequency v_0 is described by

$$\alpha(\nu - \nu_0) = \frac{p}{k_B T} \cdot S \cdot g(\nu - \nu_0), \tag{13}$$

where p is the pressure, T represents the absolute temperature, k_B is the Boltzmann's constant, S denotes the line strength of the given line and $g(v - v_0)$ is the area normalized line shape function at frequency v_0. Absorption spectroscopy can be conveniently applied for selective gas sensing, diagnostics, process and emission control and trace gas monitoring.

Usually, fundamental absorption bands in the mid-infrared region have been used in gas monitoring [143, 144]. The availability of tunable and compact diode lasers and low loss optical waveguides in the 1300 and 1500 nm regions have led to the increasing interest in the use of overtone bands which exhibit weaker transitions. The weaker absorption strength results in a reduced sensitivity and, thus, one may need to use complex multi-pass configurations or advanced measurement techniques to compensate for the reduced signal strength. In addition to the abovementioned alternatives, improved signal strength could also be obtained by exploiting the long optical path length available with PCFs.

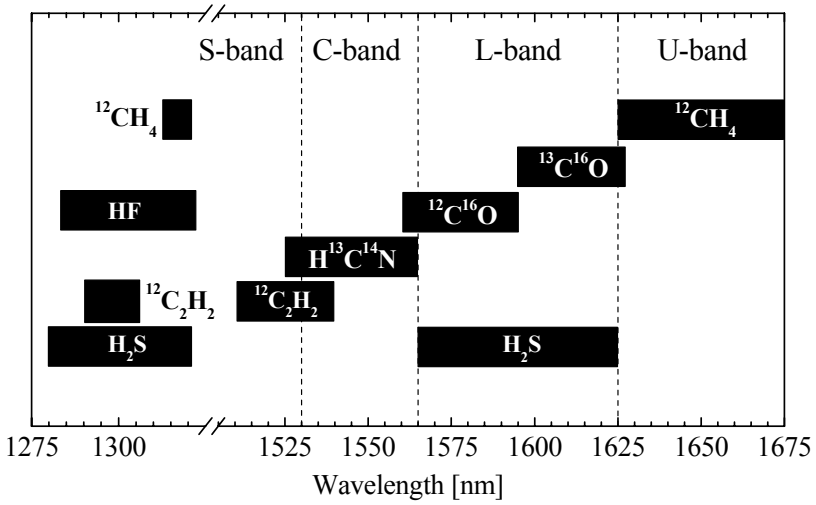

Figure 18. The wavelength ranges of the absorption spectra of several gases and optical communication bands [139-141].

5.2 Vacuum system for gas spectroscopy

A photograph of the vacuum chamber constructed for evacuation and filling of PCF samples is displayed in Fig. 19. The chamber consists of the main body made from brass and end-plates with a fiber feed through [145]. A gas inlet and an outlet for a pump were incorporated in the main body. The chamber was evacuated by utilizing a rotary pump with a pumping rate of 45 l/s. A pressure gauge and a needle valve system allowed for obtaining the desired gas pressure in the fibers. In a typical experiment, one end of a PCF was spliced to a SMF and the open end was butt-coupled to a multi-mode fiber using a V-groove for aligning the fibers. Subsequently, the fibers and the groove were placed inside the vacuum chamber. A small gap (~50 μm) between the fibers allowed for the evacuation and filling of the PCF.

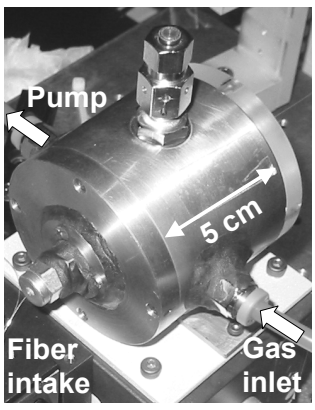

Figure 19. Vacuum chamber for evacuation and filling of fiber samples.

5.3 Supercontinuum and gas cell in a single microstructured fiber

The index-guiding mechanism and the holey structure of MFs offer a means to partially guide light in the cladding holes. The cladding holes can be filled with gases or liquids, thereby, providing a long optical interaction path between light and the fluids in the holes [12-14]. Moreover, MFs allow for an efficient SC generation due to their special dispersion and enhanced nonlinear properties. In Paper P4, both the high nonlinearity and the holey structure of MFs were exploited to combine a supercontinuum and a gas cell in a single narrow-core MF. A broadband SC was generated by launching nanosecond pulses from a compact passively Q-switched Nd:YAG laser operating at 1064 nm into an acetylene-filled MF. The basics of SC generation using ns pulses were presented in Chapter 4. The efficiency of the light-gas interaction in narrow-core MFs and potential means to enhance the strength of the absorption lines as well as the suitable molecule candidates are shortly discussed below.

Evanescent field effect in microstructured fibers

The percentage of power traveling inside the holes of MFs is a critical parameter affecting the efficiency of evanescent field devices. In order to obtain a strong light-gas interaction, a significant percentage of modal power must be located in the holes of a MF at the wavelength range of the gas absorption [12, 13]. The percentage of power effectively located within the holes (P_h) of different narrow-core MFs exhibiting a triangular cladding-hole structure and calculated using a beam propagation method [61] is displayed in Fig. 20. The corresponding characteristics of the MFs are summarized in Table 5. Also, the values of P_h at the wavelengths of 1310, 1530 and 1670 nm are presented as acetylene (1530 nm) [146] and methane (1310 and 1670 nm) [139, 147] have absorption lines near these particular wavelengths. The simulations show that an overlap of ~30% could be obtained at 1670 nm with a 1.2 micron core MF whereas the overlap reduces to less than 1% for a 4.8 micron core fiber over the whole wavelength range.

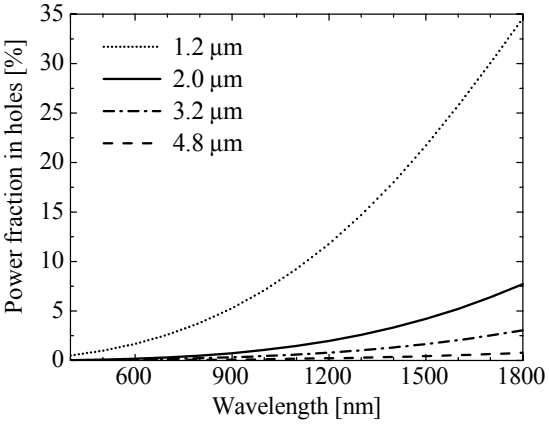

Figure 20. Percentage of power located in the holes for four MFs with different core sizes.

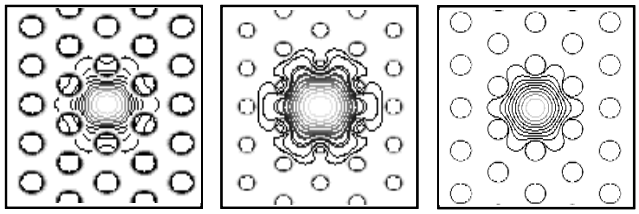

Figure 21. Simulated fundamental mode at 1500 nm for a 2.0 (left), 3.2 (middle) and 10.8 µm (right) core MF. Note different scaling.

Table 5. Characteristics of four MFs. *d*: air-hole diameter and *Λ*: pitch.

	MF-1	MF-2	MF-3	MF-4
Core size [μm]	1.2	2	3.2	4.8
***Λ* [μm]**	1	1.4	2.1	3.2
d*/*Λ	0.9	0.65	0.45	0.5
$P_{h,1310\ nm}$ **[%]**	15	2.7	1.1	0.3
$P_{h,1530\ nm}$ **[%]**	23	4.5	1.8	0.5
$P_{h,1670\ nm}$ **[%]**	29	6.1	2.4	0.6

The amount of power in the holes increases with wavelength and decreases for larger core sizes. This behavior can be explained by the facts that the mode-field diameter increases with the wavelength and that the mode sees the cladding holes for smaller air-filling fractions. The simulation of the mode-fields for MF-2 and MF-3 at 1500 nm indicates (see Fig. 21) that, for narrow-core MFs, the fundamental mode overlaps with the first ring of holes. As a comparison, a contour plot of the fundamental mode in a 10.8 micron core LMA-MF at 1500 nm is shown. In this case, the mode is well confined in the core resulting in a negligible modal overlap with the air holes which limits the use of this type of fiber for evanescent field applications.

Supercontinuum and gas cell

A typical SC spectrum generated in a 2 micron core MF filled with acetylene at a pressure of 1260 mbar is plotted in Fig. 22. The percentage of power located in the holes at 1530 nm is estimated to be around 4.5%. The SC was generated by launching ~3 ns pulses from a Nd:YAG laser at a repetition rate of 30 kHz into the MF. For an average output power of ~30 mW, the spectrum extends from 1 μm to beyond 1.7 μm. The SC light interacts with gas molecules as it is generated along the fiber giving rise to absorption lines at specific wavelengths in the spectrum. The gas-light interaction can be observed from the spectrum. The first peak close to 1390 nm corresponds to the OH-absorption whereas the second peak at 1530 nm results from acetylene absorption (resolution 10 nm). The inset shows the fine structure of the R- and P-branches of the $\nu_1 + \nu_3$ band of $^{12}C_2H_2$ observed using a higher measurement resolution of 0.1 nm. The maximum absorption line strength is ~4 dB.

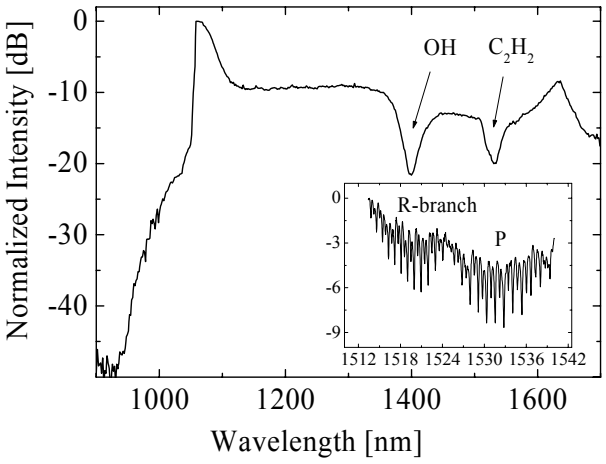

Figure 22. Supercontinuum generated in a 15 meter long 2 μm core MF filled with acetylene at 1260 mbar. Inset: Fine structure of the R- and P-branches of the $\nu_1 + \nu_3$ band of $^{12}C_2H_2$.

It is possible to improve the percentage of power located within the holes significantly by utilizing MFs with a core diameter in the order of a micrometer and an air-filling fraction of ~0.9 (MF-1). Nevertheless, the strength of the absorption line is a trade-off between the overlap and the formation of the continuum. In particular, for a given input peak power, the generation of the SC depends both on the dispersion profile and the nonlinear coefficient of the MF. As a result, the spectral components near the different absorption bands of a particular gas species are generated at the different stage of the propagation depending on the exact value of the aforementioned parameters. This in turn affects the interaction length between the light and gas and, consequently, the strength of the lines. According to Eq. (11), high dispersion values at the pump wavelength could reduce the efficiency of SC generation indicating that flat dispersion profiles and low dispersion values may be preferable. Furthermore, MFs with very small core dimensions typically exhibit two λ_{ZD}s and, therefore, a rather narrow anomalous dispersion region. Consequently, the spectral region which can be covered by the SSFS is limited and the bandwidth of the SC generated in this type of fiber may be reduced.

It is expected that the strength of the absorption lines can be enhanced by increasing the peak power of pulses or the fiber length. Furthermore, it is anticipated that the use of ps or fs pump lasers [8, 134] would result in enhanced absorption strength because of the longer interaction length, as supercontinua generated with these types of lasers are typically formed within much shorter lengths compared with ns pump lasers. However, this comes with the expense of making the system more expensive and larger.

In general, the technique can be applied to various gases absorbing at different wavelengths. A source with multiple reference bands at desired wavelengths could be realized by filling a fiber with non-reactive gases at different partial pressures chosen according to their absorption strengths and locations of the absorption bands. In other words, for a given fiber length, a higher gas pressure is usually required in the case of weakly absorbing gases. In order to extend the spectral range beyond the region covered by acetylene ($^{12}C_2H_2$, $^{13}C_2H_2$), MFs could be filled with multiple gases such as hydrogen cyanide (HCN), carbon monoxide (CO), carbon dioxide (CO_2), hydrogen sulfide (H_2S), methane (CH_4) and ethylene (C_2H_4) [139-142, 148]. Suitable reference molecules are further discussed in Section 5.5 (see also Fig. 18). Gas-filled narrow-core MFs in combination with compact lasers could provide small-sized, simple and cost-effective broadband sources that are self-referenced to the absorption lines of the gas employed. Such sources may find applications for instance in characterization of optical components and calibration of measurement instruments. In addition, the same technique could be applied to enhance the bandwidth of the SC by selecting a suitable nonlinear fluid.

5.4 Gas detection using photonic bandgap fibers

Monitoring gaseous emissions is important due to the tight environmental and health and safety regulations. Gas measurements are also used to provide feedback for different production processes to improve their efficiency. Gas detection techniques have been traditionally based on dyes that change color when exposed to gases, catalytic interactions in materials, electrochemically active materials that change their conductivity in the presence of gases, photo acoustic detection and spectroscopic techniques [149-151]. In the following, gas detection using optical waveguides, and in particular PBFs, is discussed.

The fast development of fiber optics during the last few decades has revolutionized not only the telecommunications technology but also given rise to many advances in sensing technology. Fiber-optic gas sensors offer many advantages such as immunity to electromagnetic interference, small size, low cost, light weight, resistance to high temperatures and vibrations, large bandwidth and the possibility to perform safe remote and distributed measurements [150, 152]. Different fiber and waveguide designs including fibers with a small hole in the center of the core [153], D-shaped optical fibers [154, 155], microbent optical fibers [156], hollow optical waveguides [157], fiber gratings [158], fibers and tapers with porous cladding layers [159, 160] and index-guiding MFs [12, 14, 161, 162] have been exploited in gas sensing previously. Sensors based on evanescent field effect suffer typically from a poor overlap between gas and light resulting in reduced sensitivity [154, 161] whereas hollow waveguides often exhibit high losses and multi-mode behavior [157]. Furthermore, many of the designs are complicated, difficult to fabricate and are only suitable for the detection of a single gas species. Recently, a new class of optical waveguides called air-guiding PBFs has emerged. Such fibers offer promising alternatives for a range of sensing applications due to their large overlap between the hollow-core and the mode field [163, 164], low macrobending loss [34], wide operation range [165, 166], relatively large core size [36] and low transmission loss [35]. In this section, the basic properties of hollow optical waveguides, D-shaped optical fibers and index-guiding MFs are briefly described. Moreover, the characteristics of air-guiding PBFs and the possibility of employing PBFs in gas detection are discussed.

Hollow optical waveguides

Hollow optical waveguides are usually fabricated from metal, plastic or glass tubes which are deposited with highly reflective coatings from the inside of the tubes [157]. Typically, the bore is 200 to 1000 μm in diameter. The optical and mechanical characteristics of these waveguides are generally inferior to optical fibers made from silica. In particular, such waveguides are often multi-mode and exhibit high losses limiting the practical waveguide length to a few meters. Hollow waveguides can be employed in short-distance high-power delivery and chemical sensing applications [157].

D-shaped optical fibers

Optical fibers with D-shaped cross-sections are generally manufactured by pulling the fiber from a D-shaped polished preform [155]. The flat surface of these fibers provides a direct access to the evanescent field of the light guided in the core. The sensitivity of the D-shaped optical fibers is typically only 0.1-0.2% compared with the sensitivity of an open-path gas cell [154]. Small improvements in the detection sensitivity can be obtained by coating the flat

surface with high-index films. D-shaped optical fibers find applications in distributed gas detection but are not very suitable for single-point sensing [154].

Index-guiding microstructured fibers

The gas detection sensitivity of index-guiding MFs is determined by the fractional power carried by the evanescent wave in the air holes. In general, these fibers exhibit less than 1% of the modal power in the holes but with an optimized fiber design the overlap at a particular wavelength can be ~30% (see Fig. 20). Issues affecting the modal overlap with the holes are discussed in Section 5.3. Another limitation of this type of fiber in gas sensing arises from the small-sized air holes which limit gas exchange and, thus, response times of the fibers.

Photonic bandgap fibers

In comparison to evanescent field devices [12, 153, 154, 161], the overlap between the gas and the mode field of light can be considerably improved using air-guiding PBFs [6]. As a matter of fact, such fibers can guide more than 98% of the power in the air-regions of the fiber, thus, reducing the influence of material parameters (e.g. nonlinearity, absorption, Rayleigh scattering) on the optical properties of the fiber [35, 163, 164]. By filling the holes of a PBF with gas, the fiber provides high gas detection sensitivity and a long optical path length. Moreover, only a small gas volume is required to fill the holes. The transmission band of an air-guiding PBF is typically ~100 to 200 nm wide [34], however, such fibers can exhibit multiple transmission bands and are available in a wavelength range from ~400 to 3100 nm [166]. This broad wavelength range gives potential to detect a large number of gases (see Fig. 18). Furthermore, light guidance at mid- to far-infrared wavelengths where gases exhibit stronger absorption bands may be obtained by employing special compound glasses such as chalcogenides [165]. Photonic bandgap fibers can also be integrated with more conventional fiber technology using splicing techniques and are insensitive to macrobending, which allows for the construction of compact sensing devices [34]. In addition to sensing, air-guiding PBFs could find applications in, e.g., high-power beam and short-pulse delivery [164, 167], nonlinear optics [11, 168] and particle guidance [169].

Setup for gas measurements

In Paper P5, the detection of both strongly and weakly absorbing gases using air-guiding PBFs was studied. The characteristics of the PBFs employed in the experiments are shown in Table 6. The fiber cores were formed by removing seven silica tubes from the centers of the fiber preforms. Furthermore, one end of both PBFs was spliced to a SMF for easy light coupling and improved stability.

Table 6. Characteristics of air-guiding PBFs. Λ: pitch.

	PBF-1	**PBF-2**
Core size [μm]	10	11.6
Λ [μm]	3	3.1
Length [m]	1	10
Loss [dB/m]	~ 0.2	~ 0.1
Transmission band [nm]	1400-1600	1240-1460

The absorption measurements were conducted either using a tunable laser or an LED as the light source by employing the measurement setup depicted in Fig. 23. The vacuum system and the arrangement of the fibers were described in Section 5.2. In the case of the tunable laser, the absorption spectrum was measured with a germanium photodetector and a wavemeter whereas in the LED measurements, the spectrum was recorded using an OSA. While a tunable laser provides higher measurement resolution, the use of an LED allows for faster measurements.

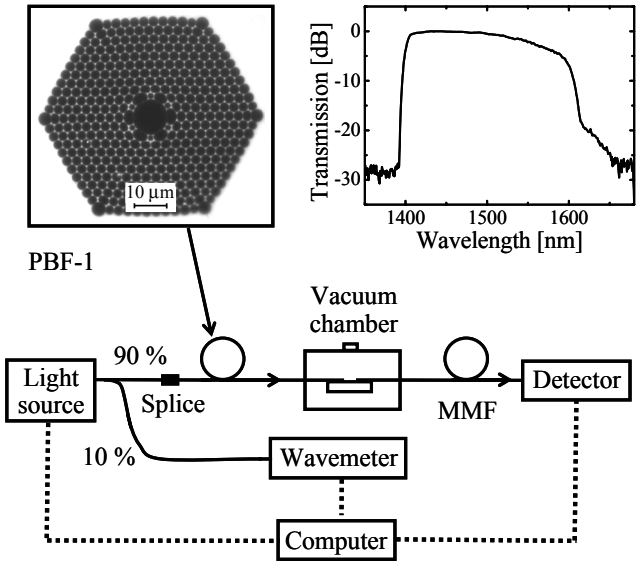

Figure 23. Experimental setup for gas detection [P5]. Normalized spectral transmission for a 3 m long PBF guiding at 1500 nm is shown in the upper right-hand corner. MMF: multi-mode fiber, PBF: photonic bandgap fiber.

Absorption measurements

By utilizing the setup depicted above, it is possible to detect gases such as acetylene (C_2H_2), hydrogen cyanide (HCN), methane (CH_4) and ammonia (NH_3) [P5, 150]. These gases are important to be monitored for, e.g., health and safety reasons. Examples of typical absorption measurements conducted using LEDs and tunable lasers as light sources are presented below.

In most cases, moderate wavelength accuracy is sufficient to identify molecular species so that an LED can be utilized as the light source to measure the absorption spectra. Figure 24a shows the R- and P-branch of the $2\nu_3$ band of $H^{13}CN$ at ~80 mbar measured using an LED and an OSA. The measurement was conducted by employing a 1 m long PBF guiding around 1500 nm. For this fiber, ~97% of power was propagating inside the core. The double branch shape seen in the figure is characteristic to the absorption spectrum of a large number of gases. Both of the branches consist of more than 20 vibration-rotation absorption lines in the 1520-1565 nm wavelength region which can be conveniently used for gas detection. The $H^{13}CN$ molecule exhibits a permanent dipole moment. The dipole moment makes the molecule prone to adhere to the walls of the glass capillaries leading to a decreasing gas pressure inside a fiber as molecules leave the gas phase [170]. A similar behavior is expected for other molecules with permanent dipole moments such as ammonia. As a consequence, the detection of these molecules may require special attention as the pressure inside the fiber may not be able to respond to variations in the pressure outside the fiber.

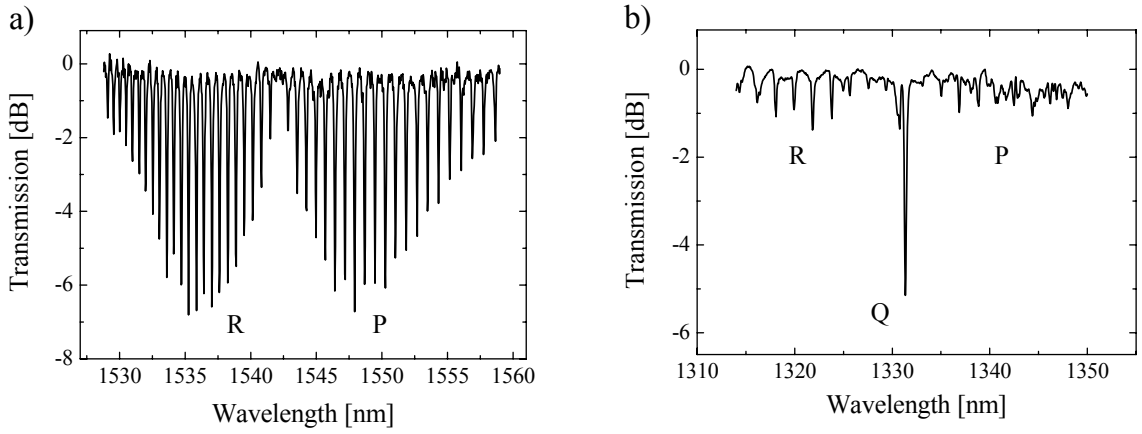

Figure 24. a) Absorption spectrum of $H^{13}CN$ at ~80 mbar in a 1 m long PBF guiding around 1500 nm. b) Absorption spectrum of CH_4 at 700 mbar in a 10 m long PBF guiding around 1300 nm.

Long path lengths are difficult to realize using conventional absorption cells as they require careful alignment and well collimated light beams. Consequently, interaction lengths in gas cells are usually limited to a few meters even when complex multi-pass cells are used. In Paper P5, it was demonstrated that PBFs also provide long enough interaction length to allow for the detection of weakly absorbing gases such as methane. A typical absorption spectrum of the R-, Q- and P-branch of $\nu_2+2\nu_3$ band of methane at 700 mbar in a 10 m long PBF is displayed in Fig. 24b. The measurement was performed using an LED and an OSA. The spectrum consists of multiplets which are not resolved in the LED measurement. The branches can, however, be partly resolved using a tunable laser [P6]. The strongest dip in the spectrum close to 1330 nm represents the Q-branch. Although the fine structure can not be fully observed from the measurement, the Q-branch feature is unique for gas detection purposes and the use of an LED will generally be sufficient.

Laser measurements allow for an improved spectral resolution and are, therefore, better suited for the detection of molecules which exhibit congested absorption spectra as is the case with for instance ammonia in the 1500 nm wavelength range. Such measurements can also be exploited to distinguish between weak absorption bands of molecules such as $^{12}C_2H_2$ which are located in the same spectral region [P6]. Figure 25a displays an absorption spectrum of the P-branch of $^{12}C_2H_2$ (10 mbar) in a 1 m long PBF measured using a tunable laser as the light source. The strongest absorption lines of the measurement exceed 25 dB and clearly show the potential of PBFs for gas detection. For comparison, a reference measurement performed using a 1 m long conventional absorption cell is displayed in Fig. 25b. Compared with the absorption cell, the fiber measurement exhibits a higher background noise which is attributed to the polarization characteristics of the fiber. In the case of the gas cell, Brewster windows eliminate the undesired interference effects. However, the use of such windows makes the cell design more complicated and requires also a careful control of the polarization of light in order to minimize coupling losses. Moreover, in the case of the PBF, the absorption line strength can be easily increased by using a longer fiber length. This is in contrast to the use of bulky multi-pass gas cells that can be cumbersome to operate.

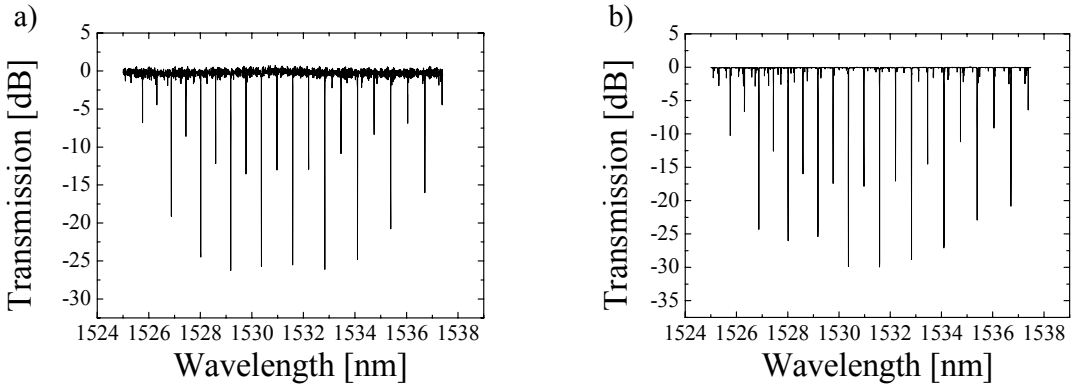

Figure 25. a) Absorption spectrum of P-branch of $^{12}C_2H_2$ in a 1 m long PBF. b) Absorption spectrum of P- branch of $^{12}C_2H_2$ in a 1 m long gas cell. Measurements were conducted at a gas pressure of 10 mbar using a tunable laser as the light source (1 pm step size).

Photonic bandgap fibers have the potential to provide compact and cost-effective sensors which can be integrated with standard fiber-optic systems using splicing techniques. Due to the low loss of PBFs and the high overlap between the mode and the gas-filled core, it is possible to obtain very long effective interaction lengths [35]. This allows for the detection of weakly absorbing gases or weak absorption lines as the absorption strength can be increased by using a longer fiber length. In practice, reflection measurements could be preferable as they require only a single transmission fiber. Air-guiding PBFs may find applications for instance in analyzing gas samples using small gas volumes and in remote gas detection. However, many issues need to be considered before the full potential of PBFs can be exploited. Although the loss of the state-of-the-art air-guiding PBFs is already low at 1500 nm region, low loss fibers do not yet widely exist for other wavelength regions. Furthermore, the polarization characteristics [171, 172] may limit the operation of PBF based devices and systems especially when long fiber lengths are required. Despite the aforementioned challenges, PBFs should offer promising opportunities for sensing applications in the near future.

5.5 Gas-filled photonic bandgap fiber as a wavelength reference

Accurate knowledge of the wavelength of an optical source is important in a number of applications in optical communications and metrology [146, 173]. Consequently, there is a need for reliable wavelength standards that can be used in the calibration of measurement instruments and for the frequency stabilization of lasers. Wavelength references are divided into absolute, also known as primary, standards (e.g. molecular references) and relative wavelength standards (e.g. Fabry-Pérot interferometer). Absolute references provide very accurate calibration wavelengths, have a very small and accurately quantified environmental sensitivity and can be reproduced anywhere in the world. Absolute references are not available in all wavelength regions and, therefore, relative references are also needed. Such references can provide tunability and reference points at arbitrary wavelengths within a broad wavelength range but are sensitive to temperature, pressure and strain and need to be calibrated against absolute references on a regular basis. To date, various devices and materials have been proposed to realize both types of references [146, 174-176].

In this Chapter, some commonly employed relative and absolute wavelength references are briefly described. Moreover, an optical wavelength reference based on a gas-filled PBF is discussed [P6]. By utilizing lock-in technique, the output frequency of a tunable laser was successfully stabilized to a number of weak absorption lines of acetylene, which coincide well with wavelength division multiplexing (WDM) channels [P6].

Fiber Bragg grating

A fiber Bragg grating is a short length of fiber exhibiting a periodic change of the refractive index of the core along its length [177]. The grating period is proportional to the reflected Bragg wavelength which can be used for reference purposes [175]. Such gratings provide cost-effective references but are usually prone towards changes in environmental conditions.

Fabry-Pérot interferometer

A Fabry-Pérot interferometer is an optical resonator which consists of two reflective surfaces [178-180]. The interference effect generates a transmission spectrum with periodic maxima that can be employed as tunable references over a broad wavelength range [179, 180].

Molecular references

Molecular absorption lines provide stable and accurate references as the wavelengths of the lines are determined by fundamental constants [146, 181]. Many parameters need to be considered when selecting molecular species for reference purposes: the location and width of the bands, number of absorption lines, strength of lines, pressure, absorption length, availability, hazards, etc. Although molecular references are very accurate, small shifts in the wavelengths and widths of the absorption lines can result from changes in pressure, temperature and electric or magnetic fields [141, 142]. In addition, Doppler-broadening increases the wavelength uncertainty of the lines. The Doppler-effect can be overcome by applying saturated absorption spectroscopy. This allows for improving the accuracy and stability by typically two orders of magnitude [146, 182, 183]. Saturated absorption is not discussed here but a few experiments have been reported using PBFs [170, 184, 185].

Wavelength references for optical telecommunications

The need for accurate, compact and cost-effective optical wavelength references is increasing as the channel spacing is reduced and the number of data carrying channels is increased in optical communication systems. The discussion below concentrates on molecular wavelength references. Molecular references are an attractive choice as there is a large number of gas species having accurately characterized absorption lines located at telecom bands and such references are typically easy to implement. The International Telecommunication Union (ITU) has designated the optical spectrum according to ITU-T SG.15. The WDM channels are specified by the ITU recommendations to operate near the gain region of erbium doped fiber amplifiers with an inter-channel spacing of 12.5, 25, 50, 100 and 200 GHz [173]. The WDM frequency grids are anchored to 193.1 THz. The recommended maximum frequency drift from the channel center is 20 GHz for the 100 GHz WDM system [186]. Extensive research has been carried out to find molecular absorption lines that coincide with the WDM channels with accuracy better than 2 GHz thus being an order of magnitude better than the maximum drift [139, 140, 146]. The wavelength ranges of the absorption spectra of various molecules in the optical communications bands are presented in Fig. 18. In order to get a good coverage of the C-band, it is possible to use gases such as acetylene ($^{12}C_2H_2$, $^{13}C_2H_2$) and hydrogen cyanide (HCN) [140]. On the other hand, to cover the L- and U-bands carbon monoxide (CO), carbon dioxide (CO_2), hydrogen sulfide (H_2S), methane (CH_4) and ethylene (C_2H_4) can be employed [139-141, 148]. Ethylene has absorption lines near 1625 nm. Consequently, these lines could be used as references for the supervisory telecom channel. Other possible molecules for the 1500 nm wavelength range are hydrogen iodide (HI), ammonia (NH_3) and hydrogen chloride (HCl) [162] whereas suitable candidates for the 1300 nm region include hydrogen fluoride (HF), hydrogen bromide (HBr) and methane (CH_4) [162]. Although many of these molecules have favorably located lines, some lines are very weak and, therefore, a long path length is required to identify them.

Wavelength reference based on a gas-filled photonic bandgap fiber

Molecular references are usually based on 5 to 20 cm long gas-filled glass cells. The gas pressure depends on the molecular species and the cell design. In general, low pressure is desired to avoid the excess pressure broadening and pressure shift of the absorption lines. Thus, for weakly absorbing molecules, one might need to increase the interaction length between light and gas in order to obtain a sufficient signal level. The optical path length can be increased by using a multi-pass configuration but it will usually be limited to around one meter when a portable wavelength reference is desired. In addition, such multi-pass cells demand careful beam control and alignment which can make the cell design complex. Therefore, to ensure an adequate strength of the absorption lines, a compromise between the gas pressure and the optical path length is to be made.

Air-guiding PBFs provide a means to efficiently exploit the interaction between light and gas in a fiber as most of the power travels in the fiber core. Due to the low loss guiding mechanism provided by PBFs and the small natural size of fibers, length and size constraints encountered with gas cells can be alleviated. Furthermore, since PBFs have relatively low bending loss, compact wavelength artifacts can be realized while at the same time only a small gas quantity is required to fill the core and cladding voids. A photograph comparing the size of a typical gas cell with that of an optical fiber is shown in Fig. 26. In the case of PBFs, the use of a low gas pressure and, consequently, reduced absorption line strength can be

compensated for by employing a longer fiber length. This provides a large selection of potential reference molecules. In Fig. 27, the absorption spectrum of a 15 cm long glass cell and a 5 m long PBF filled with $^{12}C_2H_2$ at 30 mbar and 1 mbar are presented. Measurements were conducted using a tunable laser as the light source (resolution 1 pm). The absorption lines of the fiber measurement are stronger although the gas pressure is 30 times lower. As the pressure shift and the collision broadening are proportional to the gas pressure with typical coefficients in the range of -0.2 to -0.5 MHz/mbar and ~2-10 MHz/mbar [140], respectively, the accuracy of a reference may be improved by using a PBF as a gas cell. However, compared with a conventional cell, additional collision broadening may occur in PBFs due to the relatively small core dimension [185].

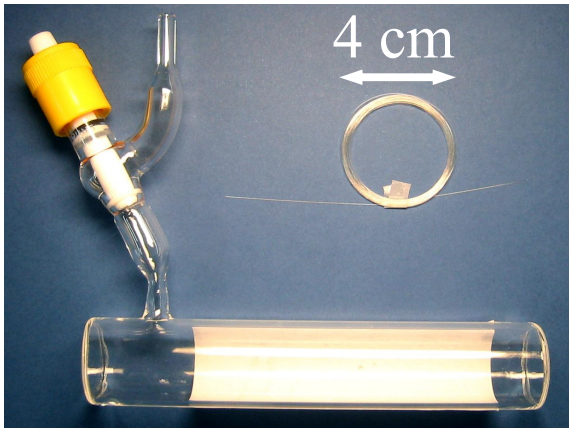

Figure 26. Photograph of a 15 cm long cell and a 5 m long fiber illustrating the small size of fiber-based devices.

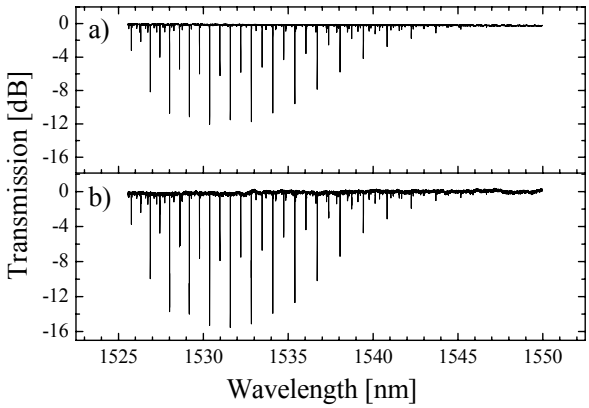

Figure 27. a) P-branch of $^{12}C_2H_2$ at 30 mbar in a 15 cm long cell. b) P-branch of $^{12}C_2H_2$ at 1 mbar in a 5 m long PBF.

In Paper P6, the use of gas-filled PBFs as optical wavelength references was investigated. The high sensitivity and long interaction length provided by PBFs allows for the use of molecules with weak absorption lines coinciding with the WDM channels. By utilizing a 5 m long PBF, four acetylene lines located within 500 to 1000 MHz from the nearest WDM channel were observed [P6]. One of the lines belongs to the $\nu_1 + \nu_3 + \nu_4^1 - \nu_4^1$ hot band and three of the lines to the $\nu_1 + \nu_3$ $^{12}C^{13}CH_2$ band of $^{12}C_2H_2$ (1.1% natural abundance of ^{13}C). To the best of our knowledge, these lines have not been suggested to be used as WDM channel references. As an example, other candidate reference lines for the ITU-channels coinciding with the mixed isotope lines are offset several GHz from the respective channel centers [186]. Three of the abovementioned lines at 20 mbar pressure measured using a tunable laser as the light source (1 pm resolution) are shown in Fig. 28. The pressure shift and broadening of the lines depend on the line number and are less than 0.1 and 2 pm, respectively, at this pressure [141, 142]. In order to exploit the full capacity of optical communication systems, it is essential that the lasers assigned for the WDM-channels stay close to the channel centers. In Paper 6, the output frequency of the external cavity laser was successfully stabilized to the center point of the abovementioned weak absorption lines coinciding with the ITU-channels. The center point was preferred instead of the slope of the absorption line as this makes the line wavelength values straightforward to compare with the literature. The laser frequency stayed within 100 MHz from the center points of the absorption lines [P6]. Consequently, these absorption lines could be exploited in the frequency stabilization of lasers to provide accurate and stable laser sources for dense WDM systems [173, 187].

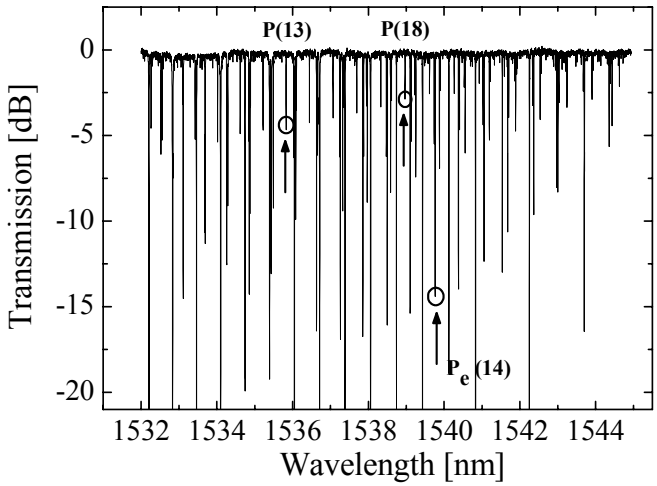

Figure 28. Absorption spectrum of acetylene at 20 mbar in a 5 m long PBF. P(13) and P(18) lines of $\nu_1 + \nu_3$ $^{12}C^{13}CH_2$ band and $P_e(14)$ line of $\nu_1 + \nu_3 + \nu_4^1 - \nu_4^1$ hot band of $^{12}C_2H_2$ (1.1% natural abundance of ^{13}C) are marked by arrows.

In order to cover the entire useful transmission band of optical fibers, references are also needed in other wavelength regions. One possible reference candidate for the 1300 nm region is methane [139]. For wavelength referencing purposes, it is important to choose a single line to obtain high accuracy. Using a 10 m long fiber guiding at 1300nm (see Table 7) and a tunable laser as the light source, a suitable single line belonging to the R-branch of the $\nu_2+2\nu_3$ combination band near 1314 nm was observed [P6]. The experiments reported in Paper P6, Ref. 188 and by Benabid *et al.* in Ref. 189 show that gas-filled PBFs are promising candidates for monitoring and calibrating channels in WDM systems, frequency stabilization of lasers and calibration of measurement instruments.

6 Summary

In this dissertation, the optical properties and novel applications of photonic crystal fibers have been investigated and developed. The first part of the thesis deals with polarization characteristics of index-guiding microstructured fibers. In Paper P1, the polarization properties of different types of birefringent microstructured fibers were studied with emphasis on the sensitivity of these characteristics to temperature and wavelength. The study indicates that in the presence of strong form birefringence, the differential group and phase delays can have very different values and their ratio can also be strongly wavelength dependent. This is often the case with narrow-core microstructured fibers which can exhibit high unintentional form birefringence. Furthermore, it was found that the relative temperature sensitivities of the phase and group birefringence for single-material narrow-core microstructured fibers are smaller by a factor of 100 and 10, respectively, compared with fibers with stress-induced birefringence. Such fibers are, thus, promising candidates for temperature insensitive sensors and interferometers whereas single-mode large mode-area microstructured fibers with stress birefringence could be useful in polarization-maintaining high-power applications. In Paper P2, the polarization-mode dispersion of large mode-area microstructured fibers was investigated. The results show that the conventional measurement techniques employed work reliably also with microstructured fibers. In addition, the polarization-mode dispersion and birefringence values comparable to the state-of-the-art single-mode fibers were observed for one microstructured fiber sample indicating an excellent symmetry in the microstructure both in the transversal and longitudinal direction of the fiber.

The second part of the thesis deals with supercontinuum generation using nanosecond pulses. In Paper P3, supercontinuum generation is demonstrated in large mode-area microstructured fibers by launching into the fibers nanosecond pulses from a passively Q-switched Nd:YAG laser. Nonlinear phenomena such as Raman scattering and four-wave mixing processes were observed to contribute to the formation of the broad spectrum. The special properties of large mode-area microstructured fibers can be exploited to provide single-mode high-power supercontinuum sources with low output beam divergence and polarization dependence. In the third part of the thesis, the possibility of employing a single acetylene-filled microstructured fiber as a gas cell and nonlinear medium for supercontinuum generation was investigated using a passively Q-switched Nd:YAG laser [P4]. The evanescent field of the light interacts with the gas located in the holes resulting in light absorption at specific wavelengths in the output spectrum. The approach provides a compact and cost-effective supercontinuum source that is self-referenced to the acetylene lines in the 1500 nm region. A small core dimension and a high air-filling fraction were found to result in efficient interaction between light and gas and, consequently, in stronger absorption lines. Such a SC source may find applications in characterization of optical components and in calibration of measurement instruments. The technique could also be applied to various gases absorbing at different wavelengths.

The third part of the work focuses also on applications based on photonic bandgap fibers. Air-guiding photonic bandgap fibers have attracted growing interest for sensor applications as they can guide more than 98% of the power in the hollow core of the fiber which can be filled with sample fluids. In this thesis, two novel photonic bandgap fiber-based devices were investigated. In Paper P5, gas detection using air-guiding photonic bandgap fibers was demonstrated. In particular, these fibers were applied to characterize absorption lines of

several gases such as acetylene and hydrogen cyanide by employing tunable lasers or LEDs as the light sources. The long interaction length and the strong light-gas interaction were found to be valuable in the detection of weakly absorbing gases such as methane. Photonic bandgap fibers could find applications in analyzing gas samples using small gas volumes and in remote gas detection. In Paper P6, a compact optical wavelength reference based on a gas-filled photonic bandgap fiber was realized. These fibers allow for the use of weak absorption lines without the need for cumbersome multi-pass absorption cells. In particular, it was demonstrated that such fibers filled with gas can provide references for optical communications and calibration purposes. Four weak absorption lines belonging to the hot and mixed isotope bands of acetylene were identified and suggested to be used as references in wavelength division multiplexing systems. The lines are located within 1 GHz from the nearest channel centers. By utilizing lock-in technique, the output frequency of a tunable external cavity laser was successfully stabilized to these weak absorption lines.

List of acronyms and symbols

BPM	Beam propagation method
DGD	Differential group delay
DUT	Device under test
DW	Dispersive wave
FA	Fixed analyzer
FWM	Four-wave mixing
HF	Holey fiber
ITU	International Telecommunication Union
JME	Jones Matrix Eigenanalysis
LED	Light emitting diode
LMA	Large mode-area
MF	Microstructured fiber
MI	Modulation instability
MMF	Multi-mode fiber
MOF	Microstructured optical fiber
OFDR	Optical frequency-domain reflectometer
OSA	Optical spectrum analyzer
PBF	Photonic bandgap fiber
PCF	Photonic crystal fiber
PMD	Polarization-mode dispersion
SC	Supercontinuum
SMF	Single-mode fiber
SRS	Stimulated Raman scattering
SSFS	Soliton self-frequency shift
WDM	Wavelength division multiplexing
XPM	Cross-phase modulation

c	speed of light in vacuum
d	hole diameter
g	area normalized line shape function
k	mode-coupling factor
k_B	Boltzmann's constant
n	refractive index
n_f	mode index of the fast polarization mode
n_s	mode index of the slow polarization mode
p	pressure

I_0	incident power
I_T	transmitted power
K_T	temperature dependence of the phase birefringence
K_τ	temperature dependence of the group birefringence
L	fiber length
L_p	path length
L_b	beat length
P_p	peak power
P_{av}	average power
P_h	power effectively located within the holes
R	bending radius
S	line strength
T	temperature

α	absorption coefficient
β	propagation constant
β_{as}	propagation constant of the anti-Stokes wave

β_f propagation constant of the fast polarization mode
β_p propagation constant of the pump
β_s propagation constant of the slow polarization mode
β_{st} propagation constant of the Stokes wave
β_2 group velocity dispersion coefficient
γ nonlinear coefficient
λ wavelength
λ_p pump wavelength
λ_{ZD} zero-dispersion wavelength
v_g group velocity
v_0 center frequency of the field
ω angular frequency
ω_{as} anti-Stokes frequency
ω_p pump frequency
ω_{st} Stokes frequency
$\Delta\beta$ phase birefringence in radians
Δn phase birefringence
$\Delta\tau_g$ differential group delay
$\Delta\tau_p$ differential phase delay
$\Delta\tau_{g,n}$ normalized differential group delay
$\Delta\tau_{p,n}$ normalized differential phase delay
$\Delta\omega$ measurement bandwidth
Λ pitch of the lattice
Ω_S frequency shift between the pump and the Stokes or anti-Stokes bands

References

[1] J. C. Knight, T. Birks, P. S. J. Russell, and D. Atkin, "All-silica single-mode optical fiber with photonic crystal cladding", *Opt. Lett*. **21**, 1547-1549 (1996), Errata *Opt. Lett.* **22**, 484-485 (1997).

[2] E. Yablonovitch, "Inhibited spontaneous emission in solid-state physics and electronics", *Phys. Rev. Lett*. **58**, 2059-2062 (1987).

[3] S. John, "Strong localization of photons in certain disordered dielectic superlattices", *Phys. Rev. Lett*. **58**, 2486-2489 (1987).

[4] J. C. Knight, J. Arriaga, T. A. Birks, A. Ortigosa-Blanch, W. J. Wadsworth, and P. St. J. Russell, "Anomalous dispersion in photonic crystal fiber", *Photonics Technol. Lett*. **12**, 807-809 (2000).

[5] T. A. Birks, J. C. Knight, and P. S. J. Russell, "Endlessly single-mode photonic crystal fiber", *Opt. Lett*. **22**, 961-963 (1997).

[6] R. F. Cregan, B. J. Mangan, J. C. Knight, T. A. Birks, P. S. J. Russell, P. J. Roberts, and D. C. Allan, "Single-mode photonic band gap guidance of light in air", *Science* **285**, 1537-1539 (1999).

[7] A. Ortigosa-Blanch, J. C. Knight, W. J. Wadsworth, J. Arriaga, B. J. Mangan, T. A. Birks, and P. S. J. Russell, "Highly birefringent photonic crystal fibers", *Opt. Lett.* **25**, 1325-1327 (2000).

[8] J. K. Ranka, R. S. Windeler, and A. J. Stentz, "Efficient visible continuum generation in air-silica microstructure optical fibers with anomalous dispersion at 800 nm", *Conference on Lasers and Electro-Optics CLEO '99*, CPD8/1-CPD8/2 (1999).

[9] C. Peucheret, B. Zsigri, P. A. Andersen, K. S. Berg, A. Tersigni, P. Jeppesen, K. P. Hansen, and M. D. Nielsen, "40 Gbit/s transmission over photonic crystal fibre using mid-span spectral inversion in highly nonlinear photonic crystal fibre", *Electron. Lett.* **39**, 919-921 (2003).

[10] B. Zsigri, C. Peucheret, M. D. Nielsen, and P. Jeppesen, "Transmission over 5.6 km large effective area and low-loss (1.7 dB/km) photonic crystal fibre", *Electron. Lett.* **39**, 796-798 (2003).

[11] F. Benabid, J. C. Knight, G. Antonopoulos, and P. St. J. Russell, "Stimulated Raman scattering in hydrogen-filled hollow-core photonic crystal fiber", *Science* **298**, 399-402 (2002).

[12] T. M. Monro, W. Belardi, K. Furusawa, J. C. Baggett, N. G. R. Broderick, and D. J. Richardson, "Sensing with microstructured optical fibres", *Meas. Sci. Technol.* **12**, 854-858 (2001).

[13] J. M. Fini, "Microstructure fibres for optical sensing in gases and liquids", *Meas. Sci. & Tech.* **15**, 1120-1128 (2004).

[14] Y. L. Hoo, W. Jin, C. Li, H. L. Ho, D.Wang, and R. S. Windeler, "Evanescent-wave gas sensing using microstructure fiber," *Opt. Eng.* **41**, 8-9 (2002).

[15] J. Jensen, P. Hoiby, G. Emiliyanov, O. Bang, L. Pedersen, and A. Bjarklev, "Selective detection of antibodies in microstructured polymer optical fibers", *Opt. Express* **13**, 5883-5889 (2005).

[16] J. Limpert, T. Schreiber, S. Nolte, H. Zellmer, A. Tünnermann, R. Iliew, F. Lederer, J. Broeng, G. Vienne, A. Petersson, and C. Jakobsen, "High-power air-clad large-mode-area photonic crystal fiber laser", *Opt. Express* **11**, 818-823 (2003).

[17] S. A. Diddams, D. J. Jones, J. Ye, S. T. Cundiff, J. L. Hall, J. K. Ranka, R. S. Windeler, R. Holzwarth, T. Udem, and T. W. Hänsch, "Direct link between microwave and optical frequencies with a 300 THz femtosecond laser comb", *Phys. Rev. Lett.* **84**, 5102-5105 (2000).

[18] J. C. Knight, T. A. Birks, R. F. Cregan, P. S. J. Russell, and J.-P. de Sandro, "Large mode area photonic crystal fibre", *Electron. Lett.* **34**, 1347-1348 (1998).

[19] M. Lehtonen, G. Genty, and H. Ludvigsen, "Absorption and transmission spectral measurements of fiber-optic components using supercontinuum radiation", *Appl. Phys. B-Lasers Opt.* **81**, 231–234 (2005).

[20] M. Lehtonen, "Applications of microstructured fibers: Supercontinua and novel components", *Doctoral dissertation*, *Helsinki University of Technology* (2005).

[21] I. Hartl, X. D. Li, C. Chudoba, R. K. Ghanta, T. H. Ko, J. G. Fujimoto, J. K. Ranka, R. S. Windeler, "Ultrahigh-resolution optical coherence tomography using continuum generation in an air-silica microstructure optical fiber", *Opt. Lett.* **26**, 608-610 (2001).

[22] B. Povazay, K. Bizheva, A. Unterhuber, B. Hermann, H. Sattmann, A. F. Fercher, W. Drexler, A. Apolonski, W. J. Wadsworth, J. C. Knight, P. S. J. Russell, M. Vetterlein, and E. Scherzer, "Submicrometer axial resolution optical coherence tomography", *Opt. Lett.* **27**, 1800-1802 (2002).

[23] H. Takara, T. Ohara, K. Mori, K. Sato, E. Yamada, Y. Inoue, T. Shibata, M. Abe, T. Morioka, and K. I. Sato, "More than 1000 channel optical frequency chain generation from single supercontinuum source with 12.5 GHz channel spacing", *Electron Lett.* **36**, 2089-2090 (2000).

[24] P. V. Kaiser, E. A. J. Marcatili, and S. E. Miller, "A new optical fiber", *Bell Syst. Tech. J.* **52**, 265-269 (1973).

[25] A. Bjarklev, J. Broeng, and A. S. Bjarklev, "Photonic Crystal Fibres", *Kluwer Academic Publishers Boston* (2003).

[26] T. A. Birks, P. J. Roberts, P. St. J. Russell, D. M. Atkin, and T. J. Shepherd, "Full 2-D photonic bandgaps in silica/air structures", *Electron. Lett.* **31**, 1941-1943 (1995).

[27] P. Russell, "Photonic crystal fibers", *Science* **299**, 358-362 (2003).

[28] J. C. Knight, J. Broeng, T. A. Birks, and P. S. J. Russell, "Photonic band gap guidance in optical fibers", *Science* **282**, 1476-1478 (1998).

[29] D. Kominsky, G. Pickrell, and R. Stolen, "Generation of random-hole optical fiber", *Opt. Lett.* **28**, 1409-1411 (2003).

[30] F. Luan, A. K. George, T. D. Hedley, G. J. Pearce, D. M. Bird, J. C.Knight, P. St. J. Russell, "All solid photonic bandgap fiber", *Opt. Lett.* **29**, 2369-2371 (2004).

[31] G. P. Agrawal, "Nonlinear Fiber Optics", Third edition, *Academic Press San Diego* (2001).

[32] X. Chen, M. Li, N. Venkataraman, M. T. Gallagher, W. A. Wood, A. M. Crowley, J. P. Carberry, L. A. Zenteno, and K. W. Koch, "Highly birefringent hollow-core photonic bandgap fiber", *Opt. Express*, **12**, 3888–3893 (2004).

[33] C. M. Smith, N. Venkataraman, M. T. Gallagher, D. Müller, J. A. West, N. F. Borrelli, D. C. Allan, and K. W. Koch, "Low-loss hollow-core silica/air photonic bandgap fibre", *Nature* **424**, 657–659 (2003).

[34] T. P. Hansen, J. Broeng, C. Jakobsen, G. Vienne, H. R. Simonsen, M. D. Nielsen, P. M. W. Skovgaard, J. R. Folkenberg, and A. Bjarklev, "Air-guiding photonic bandgap fibers: Spectral properties, macrobending loss and practical handling", *J. Lightwave Technol*. **22**, 11-15 (2004).

[35] P. J. Roberts, F. Couny, H. Sabert, B. J. Mangan, D. P. Williams, L. Farr, M. W. Mason, A. Tomlinson, T. A. Birks, J. C. Knight, and P. S. J. Russell, "Ultimate low loss of hollow-core photonic crystal fibres", *Opt. Express* **13**, 236-244 (2005).

[36] L. Michaille, D. M. Taylor, C. R. Bennett, T. J. Shepherd, C. Jacobsen, and T. P. Hansen, "Damage threshold and bending properties of photonic crystal and photonic band-gap optical fibres", *Conference on Defence & Security SPIE*, 30-38 (2004).

[37] T. M. Monro, Y. D. West, D. W. Hewak, N. G. R. Broderick, and D. J. Richardson, "Chalcogenide holey fibres," *Electron. Lett.* **36,** 1998-2000 (2000).

[38] V. V. R. K. Kumar, A. K. George, J. C. Knight, and P. S. J. Russell, "Tellurite photonic crystal fiber," *Opt. Express* **11**, 2641-2645 (2003).

[39] H. Ebendorff-Heidepriem, P. Petropoulos, S. Asimakis, V. Finazzi, R. C. Moore, K. Frampton, F. Koizumi, D. J. Richardson, and T. M. Monro, "Bismuth glass holey fibers with high nonlinearity", *Opt. Express* **12**, 5082-5087 (2004).

[40] E. Rave, P. Ephrat, M. Goldberg, E. Kedmi, and A. Katzir, "Silver halide photonic crystal fibers for the middle infrared", *Appl.Opt.* **43**, 2236-2241 (2004).

[41] A. Argyros, M. van Eijkelenborg, M. Large, and I. Bassett, "Hollow-core microstructured polymer optical fiber", *Opt. Lett.* **31**, 172-174 (2006).

[42] V. V. R. K. Kumar, A. K. George, W. H. Reeves, J. C. Knight, P. S. J. Russell, F. G. Omenetto, and A. J. Taylor, "Extruded soft glass photonic crystal fiber for ultrabroad supercontinuum generation", *Opt. Express* **10**, 1520-1525 (2002).

[43] V. L. Kalashnikov, E. Sorokin, S. Naumov, I. T. Sorokina, V. V. R. K. Kumar, and A. K. George, "Low-threshold supercontinuum generation from an extruded SF6PCF using a compact Cr4+: YAG laser", *Appl. Phys. B-Lasers Opt.* **79**, 591-596 (2004).

[44] H. Hundertmark, D. Kracht, D. Wandt, C. Fallnich, V. V. R. K. Kumar, A. K. George, J. C. Knight, and P. S. J. Russell, "Supercontinuum generation with 200 pJ laser pulses in an extruded SF6 fiber at 1560 nm", *Opt. Express* **11**, 3196-3201 (2003).

[45] K. M. Kiang, K. Frampton, T. M. Monro, R. Moore, J. Tucknott, D. W. Hewak, D. J. Richardson, and H. N. Rutt, "Extruded single-mode non-silica glass holey optical fibres", *Electron. Lett.* **38**, 546-547 (2002).

[46] M. van Eijkelenborg, M. Large, A. Argyros, J. Zagari, S. Manos, N. A. Issa, I. M. Bassett, S. C. Fleming, R. C. McPhedran, C. M. de Sterke, and N. A. P. Nicorovici, "Microstructured polymer optical fibre", *Opt. Express* **9**, 319-327 (2001).

[47] G. Barton, M. A. van Eijkelenborg, G. Henry, M. C. J. Large, and J. Zagari, "Fabrication of microstructured polymer optical fibres", *Opt. Fiber Tech*. **10**, 325-335 (2004).

[48] T. P. Hansen, J. Broeng, S. E. B. Libori, E. Knudsen, A. Bjarklev, J. R. Jensen, and H. Simonsen, "Highly birefringent index-guiding photonic crystal fibers", *Photonics Technol. Lett.* **13**, 588-590 (2001).

[49] J. Zhou, K. Tajima, K. Nakajima, K. Kurokawa, C. Fukai, T. Matsui, and I. Sankawa, "Progress on low loss photonic crystal fibers", *Opt. Fiber Technol.* **11**, 101-110 (2005).

[50] G. P. Agrawal, "Fiber-Optic Communication Systems", Second Edition, *John Wiley & Sons New York* (1997).

[51] Y. Xu, and A. Yariv, "Loss analysis of air-core photonic crystal fibers", *Opt. Lett.* **28,** 1885-1887 (2003).

[52] B. J. Mangan, L. Farr, A. Langford, P. J. Roberts, D. P. Williams, F. Couny, M. Lawman, M. Mason, S. Coupland, R. Flea, H. Sabert, T. A. Birks, J. C. Knight, and P. S. J. Russell, "Low loss (1.7 dB/km) hollow core photonic bandgap fiber", *Conference on Optical Fiber Communications OFC'04*, PDP24 (2004).

[53] D. Derickson, "Fiber Optic test and Measurement"*, Prentice Hall, New Jersey* (1998).

[54] A. Ortigosa-Blanch, A. Diez, M. Delgado-Pinar, J. L. Cruz, and M. V. Andres, "Ultrahigh birefringent nonlinear microstructured fiber", *Photonics Technol. Lett.* **16**, 1667-1669 (2004).

[55] T. A. Birks, D. Mogilevtsev, J. C. Knight, and P. S. J. Russell, "Dispersion compensation using single material fibers", *Photonics Technol. Lett.* **11**, 674-676 (1999).

[56] C. J. S. de Matos, J. R. Taylor, T. P. Hansen, K. P. Hansen, and J. Broeng, "All-fiber chirped pulse amplification using highly-dispersive air-core photonic bandgap fiber", *Opt. Express* **11**, 2832–2837 (2003).

[57] A. Ferrando, E. Silvestre, J. J. Miret, J. A. Monsoriu, M. V. Andres, and P. S. J. Russell, "Designing a photonic crystal fibre with flattened chromatic dispersion", *Electron. Lett.* **35**, 325-327 (1999).

[58] A. Ferrando, E. Silvestre, J. J. Miret, and P. Andres, "Nearly zero ultraflattened dispersion in photonic crystal fibers", *Opt. Lett.* **25**, 790-792 (2000).

[59] W. H. Reeves, J. C. Knight, P. S. J. Russell, and P. J. Roberts, "Demonstration of ultra-flattened dispersion in photonic crystal fibers", *Opt. Express* **10**, 609-613 (2002).

[60] M. Frosz, P. Falk, and O. Bang, "The role of the second zero-dispersion wavelength in generation of supercontinua and bright-bright soliton-pairs across the zero-dispersion wavelength", *Opt. Express* **13**, 6181-6192 (2005).

[61] D. Yevick and B. Hermansson, "Efficient beam propagation techniques", *IEEE J. Quantum Electron*. **26,** 109-112 (1990).

[62] N. A. Mortensen, "Effective area of photonic crystal fibers", *Opt. Express* **10**, 341-348 (2002).

[63] N. G. R. Broderick, T. M. Monro, P. J. Bennett, and D. J. Richardson, "Nonlinearity in holey optical fibers: measurement and future opportunities", *Opt. Lett.* **24**, 1395-1397 (1999).

[64] T. M. Monro, D. J. Richardson, N. G. R. Broderick, and P. J. Bennett, "Holey optical fibers: An efficient modal model", *J. Lightwave Technol.* **17**, 1093-1102 (1999).

[65] M. Koshiba, and K. Saitoh, "Structural dependence of effective area and mode field diameter for holey fibers", *Opt. Express* **11**, 1746-1756 (2003).

[66] G. Genty, T. Ritari, and H. Ludvigsen, "Generation of wide supercontinuum in a weakly nonlinear microstructured fiber", *Conference on Lasers and Electro-Optics CLEO '06*, CFK7 (2006).

[67] C. D. Poole, R. E. Wagner, "Phenomenological approach to polarisation dispersion in long single-mode fibres", *Electron. Lett.* **22**, 1029-1030 (1986).

[68] C. D. Poole and J. Nagel, "Optical Fiber Telecommunications IIIa", *Academic Press, San Diego* (1997).

[69] I. P. Kaminow, "Polarization in Optical Fibers", *IEEE J. Quantum Electron.* **17**, 15-22 (1981).

[70] J. P. Elbers, C. Glingener, M. Duser, E. Voges, "Modelling of polarization mode dispersion in singlemode fibers", *Electron. Lett.* **33**, 1894-1895 (1997).

[71] C. D. Poole, D. L. Favin, "Polarization-mode dispersion measurements based on transmission spectra through a polarizer", *J. Lightwave Technol.* **12**, 917-929 (1994).

[72] A. Galtarossa, G. Gianello, C. G. Someda, M. Schiano", In-field comparison among polarization-mode dispersion measurement techniques", *J. Lightwave Technol.* **14**, 42-49 (1996).

[73] N. Gisin, J.-P. Von der Weid, J.-P. Pellaux, "Polarization mode dispersion of short and long single-mode fibers", *J. Lightwave Technol.* **9**, 821-827 (1991).

[74] N. Gisin, B. Gisin, J.-P. Von der Weid, R. Passy, "How accurately can one measure a statistical quantity like polarization-mode dispersion?", *Photonics Technol. Lett*. **8**, 1671-1673 (1996).

[75] B. L. Heffner, "Automated measurement of polarization mode dispersion using Jones matrix eigenanalysis", *Photonics Technol. Lett*. **4**, 1066-1069 (1992).

[76] Y. Namihira, J. Maeda, "Comparison of various polarisation mode dispersion measurement methods in optical fibres", *Electron. Lett.* **28**, 2265-2266 (1992).

[77] G. J. Foschini, and C. D. Poole, "Statistical theory of polarization dispersion in single mode fibers", *J. Lightwave Technol.* **9**, 1439-1456 (1991).

[78] B. Huttner, J. Reecht, N. Gisin, R. Passy, and J. P. Von der Weid, "Local birefringence measurements in singlemode fibers with coherent frequency-domain reflectometry", *Photon. Technol. Lett.* **10**, 1458-1460 (1998).

[79] M. Wegmuller, M. Legré, and N. Gisin, "Distributed beatlength measurement in single-mode fibers with optical frequency-domain reflectometry", *J. Lightwave Tech.* **20**, 828-835, (2002).

[80] R. E. Schuh, E. S. R. Sikora, N. G. Walker, A. S. Siddiqui, L. M. Gleeson, and D. H. O. Bebbington, "Theoretical analysis and measurement of effects of fiber twist on polarization mode dispersion of optical fibers", *Electron. Lett.* **31**, 1772-1773 (1995).

[81] M. Legré, M. Wegmuller, and N. Gisin, "Investigation of the ratio between phase and group birefringence in optical single-mode fibers", *J. Lightwave Tech.* **21**, 3374-3378 (2003).

[82] M. Steel, T. White, C. Martijn de Sterke, R. McPhedran, and L. Botten, "Symmetry and degeneracy in microstructured optical fibers", *Opt. Lett.* **26**, 488-490 (2001).

[83] R. B. Dyott, "Elliptical fiber waveguides", *Artech House* (1995).

[84] J. Noda, K. Okamoto, and Y. Sasaki, "Polarization-maintaining fibers and their applications", *J. Lightwave Technol.* **LT-4**, 1071-1088 (1986).

[85] A.J. Barlow and D.N. Payne, "The stress-optic effect in optical fibres", *IEEE J. Quantum Electron.* **19**, 834-839 (1983).

[86] A. W. Snyder, and J. D. Love, "Optical Waveguide Theory", *Chapman & Hall, New York* (1983).

[87] K. Suzuki, H. Kubota, S. Kawanishi, M. Tanaka, and M. Fujita, "Optical properties of a low-loss polarization-maintaining photonic crystal fiber", *Opt. Express* **9**, 676-680 (2001).

[88] M. J. Steel, and R. M. Osgood, "Elliptical-hole photonic crystal fibers", *Opt. Lett*. **26**, 229-231 (2001).

[89] C. L. Zhao, C. Lu, X. Q. Zhou, X. F. Yang, P. R. Chaudhuri, X. Y. Wang, J. J. Lou, L. Oin, and C. Qing, "Asymmetric core photonic-crystal fibers with high birefringence", *Microwave Opt. Technol. Lett.* **42**, 498-500 (2004).

[90] G. Kakarantzas, A. Ortigosa-Blanch, T. A. Birks, P. S. J. Russell, L. Farr, F. Couny, and B. J. Mangan, "Structural rocking filters in highly birefringent photonic crystal fiber", *Opt. Lett*. **28**, 158-160 (2003).

[91] C. Kerbage, P. Steinvurzel, P. Reyes, P. S. Westbrook, R. S. Windeler, A. Hale, and B. J. Eggleton, "Highly tunable birefringent microstructured optical fiber", *Opt. Lett.* **27**, 842-844 (2002).

[92] J. R. Folkenberg, M. D. Nielsen, N. A. Mortensen, C. Jakobsen, and H. R. Simonsen, "Polarization maintaining large mode area photonic crystal fiber", *Opt. Express* **12**, 956-960 (2004).

[93] H. Kubota, S. Kawanishi, S. Koyanagi, M. Tanaka, and S. Yamaguchi, "Absolutely single polarization photonic crystal fiber", *Photon. Technol. Lett.* **16**, 182-184 (2004).

[94] A. Michie, J. Canning, K. Lyytikäinen, M. Åslund, and J. Digweed, "Temperature independent highly birefringent photonic crystal fibre", *Opt. Express* **12**, 5160-5165 (2004).

[95] M. Lehtonen, G. Genty, M. Kaivola, and H. Ludvigsen, "Supercontinuum generation in a highly birefringent microstructured fiber", *Appl. Phys. Lett.* **82**, 2197-2199 (2003).

[96] K. Saitoh, and M. Koshiba, "Photonic bandgap fibers with high birefringence", *Photonics Technol. Lett*. **14**, 1291-1293 (2002).

[97] G. Statkiewicz, T. Martynkien, and W. Urbanczyk, "Measurements of modal birefringence and polarimetric sensitivity of the birefringent holey fiber to hydrostatic pressure and strain", *Opt. Commun.* **241**, 339-348 (2004).

[98] M. Antkowiak, R. Kotynski, T. Nasilowski, P. Lesiak, J. Wojcik, W. Urbanczyk, F. Berghmans, and H. Thienpont, "Phase and group modal birefringence of triple-defect photonic crystal fibres", *J. Opt. A: Pure Appl. Opt.* **7**, 763-766 (2005).

[99] S. B. Libori, J. Broeng, E. Knudsen, A. Bjarklev, and H. R. Simonsen, "High-birefringent photonic crystal fiber," *Conference on Optical Fiber Communication OFC'01*, TuM2-1 (2001).

[100] A. Peyrilloux, T. Chartier, A. Hideur, L. Berthelot, G. Mélin, S. Lempereur, D. Pagnoux, and P. Roy, "Theoretical and experimental study of the birefringence of a photonic crystal fiber", *J. Lightwave Tech*. **21**, 536-539, (2002).

[101] T. Nasilowski, P. Lesiak, R. Kotynski, M. Antkowiak, A. Fernandez, F. Berghmans, and H. Thienpont, "Birefringent photonic crystal fiber as a multi-parameter sensor", *Symposium of Laser & Electro-Optics Society LEOS'03*, 29-32 (2003).

[102] M. Szpulak, T. Martynkien, W. Urbanczyk, J. Wójcik, and W. J. Bock, "Influence of temperature on birefringence and polarization mode dispersion in photonic crystal fibers," *International Conference on Transparent Optical Networks ICTON'02*, WeP10 (2002).

[103] M. Szpulak, T. Martynkien, and W. Urbanczyk, "Effects of hydrostatic pressure on phase and group modal birefringence in microstructured holey fibers", *Appl. Opt*. **43**, 4739-4744 (2004).

[104] D. Kim and J. U. Kang, "Sagnac loop interferometer based on polarization maintaining photonic crystal fiber with reduced temperature sensitivity", *Opt. Express* **12,** 4490-4495 (2004).

[105] C. Zhao, X. Yang, C. Lu, W. Jin, and M. S. Demokan, "Temperature-insensitive interferometer using a highly birefringent photonic crystal fiber loop mirror", *Photonics Technol. Lett*. **16,** 2535-2537 (2004).

[106] T. Schreiber, F. Röser, O. Schmidt, J. Limpert, R. Iliew, F. Lederer, A. Petersson, C. Jacobsen, K. P. Hansen, J. Broeng, and A. Tünnermann, "Stress-induced single-polarization single-transverse mode photonic crystal fiber with low nonlinearity", *Opt. Express* **13,** 7621-7630 (2005).

[107] N. Mortensen, M. Nielsen, J. Folkenberg, A. Petersson, and H. Simonsen, "Improved large-mode-area endlessly single-mode photonic crystal fibers", *Opt. Lett.* **28**, 393-395 (2003).

[108] M. D. Nielsen and N. A. Mortensen, "Photonic crystal fiber design based on the V-parameter", *Opt. Express* **11**, 2762-2768 (2003).

[109] M. Fuochi, J. R. Hayes, K. Furusawa, W. Belardi, J. C. Baggett, T. M. Monro, and D. J. Richardson, "Polarization mode dispersion reduction in spun large mode area silica holey fibres", *Opt. Express* **12,** 1972-1977 (2004).

[110] E. Suhir, "Mechanical approach to the evaluation of the low temperature threshold of added transmission losses in single-coated optical fibers", *J. Lightwave Technol.* **8** 863-868 (1990).

[111] R. R. Alfano, "The Supercontinuum Laser Source", *Springer-Verlag New York* (1989).

[112] R. R. Alfano and S. L. Shapiro, "Emission in the region 4000 to 7000 Å via four-photon coupling in glass", *Phys. Rev. Lett.* **24**, 584-587 (1970).

[113] W. Lee Smith, P. Liu, and N. Bloembergen, "Superbroadening in H2O and D2O by self-focused picosecond pulses from a YAlG:Nd laser", *Phys. Rev. A* **15**, 2396-2403 (1977).

[114] R. L. Fork, C. V. Shank, C. Hirlimann, R. Yen, and W. J. Tomlinson, "Femtosecond white-light continuum pulses", *Opt. Lett.* **8**, 1-3 (1983).

[115] P. L. Baldeck and R. R. Alfano, "Intensity effects on the stimulated four photon spectra generated by picosecond pulses in optical fibers", *J. Lightwave Technol.* **5**, 1712-1715 (1987).

[116] B. P. Nelson, D. Cotter, K. J. Blow, and N. J. Doran, "Large nonlinear pulse broadening in long lengths of monomode fiber", *Opt. Commun.* **48**, 292-294 (1983).

[117] G. Genty, M. Lehtonen, H. Ludvigsen, J. Broeng, and M. Kaivola, "Spectral broadening of femtosecond pulses into continuum radiation in microstructured fibers", *Opt. Express* **10**, 1083-1098 (2002).

[118] G. Genty, "Supercontinuum generation in microstructured fibers and novel optical measurement techniques", *Doctoral Dissertation*, *Helsinki University of Technology* (2004).

[119] J. K. Ranka, R. S. Windeler, and A. J. Stentz, "Visible continuum generation in air-silica microstructure optical fibers with anomalous dispersion at 800 nm", *Opt. Lett.* **25**, 25-27 (2000).

[120] T. A. Birks, W. J. Wadsworth, and P. St. J. Russell, "Supercontinuum generation in tapered fibers", *Opt. Lett.* **25**, 1415-1417 (2000).

[121] S. T. Cundiff, J. Ye, and J. L. Hall, "Optical frequency synthesis based on mode-locked lasers", *Rev. Sci. Instrum.* **72**, 3749-3771 (2001).

[122] K. Mori, T. Morioka, and M. Saruwatari, "Ultrawide spectral range group velocity dispersion measurement utilizing supercontinuum in an optical fiber pumped by a 1.5 μm compact laser source", *IEEE Trans. Instrum. Meas.* **44**, 712-715 (1995).

[123] S. C. Buchter, M. Kaivola, and H. Ludvigsen, "Compact, spectrally smooth, nanosecond infrared continuum source with 700 nm bandwidth", *Optical Fiber Communication Conference OFC'04,* ThA7 (2004).

[124] S. Coen, A. Hing Lun Chau, R. Leonhardt, J. D. Harvey, J. C. Knight, W. J. Wadsworth, and P. St. J. Russell, "White-light supercontinuum generation with 60-ps pump pulses in a photonic crystal fiber", *Opt. Lett.* **26**, 1356-1358 (2001).

[125] W. J. Wadsworth, N. Joly, J. C. Knight, T. A. Birks, F. Biancalana, and P. S. J. Russell, "Supercontinuum and four-wave mixing with Q-switched pulses in endlessly single-mode photonic crystal fibres", *Opt. Express* **12**, 299-309 (2004).

[126] C. V. Raman, "A new radiation", *Indian J. Phys.* **2**, 387 (1928).

[127] R. H. Stolen, Clinton Lee, and R. K. Jain, "Development of the stimulated Raman spectrum in single-mode silica fibers", *J. Opt. Soc. Am. B* **1**, 652-657 (1984).

[128] A. K. Abeeluck and C. Headley, "Continuous-wave pumping in the anomalous- and normal-dispersion regimes of nonlinear fibers for supercontinuum generation", *Opt. Lett.* **30**, 61-63 (2005).

[129] A. K. Abeeluck, C. Headley, and C. G. Jørgensen "High-power supercontinuum generation in highly nonlinear, dispersion-shifted fibers by use of a continuous-wave Raman fiber laser", *Opt. Lett*. **29**, 2163-2165 (2004).

[130] F. M. Mitschke, and L. F. Mollenauer, "Discovery of the soliton self-frequency shift", *Opt. Lett.* **11**, 659-661 (1986).

[131] N. Akhmediev, and M. Karlsson, "Cherenkov radiation emitted by solitons in optical fibers", *Phys. Rev. A* **51**, 2602-2607 (1995).

[132] J. M. Dudley, L. Provino, N. Grossard, H. Maillotte, R. S. Windeler, B. J. Eggleton, and S. Coen, "Supercontinuum generation in air-silica microstructured fibers with nanosecond and femtosecond pulse pumping", *J. Opt. Soc. Am. B-Opt. Phys.* **19**, 765-771 (2002).

[133] E.A. Golovchenko, P. V. Mamyshev, A. N. Pilipestskii, and E. M. Dianov, "Mutual influence of the parametric effects and stimulated Raman scattering in optical fibers", *J. Quantum Electron*. **26**, 1815-1820 (1990).

[134] G. Genty, M. Lehtonen, and H. Ludvigsen, "Effect of cross-phase modulation on supercontinuum generated in microstructured fibers with sub-30 fs pulses", *Opt. Express* **12**, 4614-4624 (2004).

[135] B. C. Stuart, M. D. Feit, A. M. Rubenchik, B. W. Shore, and M. D. Perry, "Laser-Induced Damage in Dielectrics with Nanosecond to Subpicosecond Pulses", *Phys. Rev. Lett.* **74***,* 2248–2251 (1995).

[136] S. Wilcox, L. C. Botten, C. M. de Sterke, B. T. Kuhlmey, R. C. McPhedran, D. P. Fussell, and S. Tomljenovic-Hanic, *"*Long wavelength behavior of the fundamental mode in microstructured optical fibers*"*, *Opt. Express* **13,** 1978-1984 (2005).

[137] M. D. Nielsen, C. Jacobsen, N. A. Mortensen, J. R. Folkenberg, and H. R. Simonsen, "Low-loss photonic crystal fibers for transmission systems and their dispersion properties", *Opt. Express* **12,** 1372-1376 (2004).

[138] K. J. Blow and D. Wood, "Theoretical description of transient stimulated Raman scattering in optical fibers", *IEEE J. Quantum Electron.* **25**, 2665 (1989).

[139] T. Dennis*,* E. A. Curtis, C. W. Oates, L. Hollberg*,* and S. L. Gilbert, "Wavelength references for 1300-nm wavelength-division multiplexing", *J. Lightwave Technol.* **20**, 804-810 (2002).

[140] J. C. Petersen, and J. Henningsen, "Molecules as absolute standards for optical telecommunications. Requirements and characterization", *International Union of Radio Sciency URSI'02,* paper 1777 (2002).

[141] Dennis, S.L. Gilbert, and W.C. Swann, "Wavelength references for wavelength division multiplexing", *Contemporary Photonic Technologies Workshop* 143-146 (2001).

[142] M. Kusaba and J. Henningsen, "The $\nu_1 + \nu_3$ and the $\nu_1 + \nu_2 + \nu_4^1 + \nu_5^{-1}$ combination bands of $^{13}C_2H_2$. Linestrengths, broadening parameters, and pressure shifts", *J. Mol. Spec.* **209**, 216-227 (2001).

[143] A. Ólafsson, and J. Henningsen, "Intraline tunable CO_2 waveguide lasers and applications in high resolution spectroscopy", *Infrared Phys. & Technol.* **36**, 309-319 (1995).

[144] H. De Vries, M. Van Lieshout, F. J. M. Harren, and J. Reuss, "IR laser trace gas detection applied to environmental and biological problems" *Infrared Phys. & Technol.* **36**, 483-488 (1995).

[145] E. R. I. Abraham and E. A. Cornell, "Teflon feedthrough for coupling optical fibers into ultrahigh vacuum systems", *Appl. Opt*. **37**, 1762-1763 (1998).

[146] K. Nakagawa, M. de Labachelerie, Y. Awaji, and M. Kourogi, "Accurate optical frequency atlas of the 1.5 μm bands of acetylene", *J. Opt. Soc. Am. B* **13**, 2708 (1996).

[147] K. Ikuta, Y. Oki, and N. J. Vasa, "Remote sensing of methane differential absorption lidar at 1.67μm", *Conference on Lasers and Electro-optics CLEO'98,* CTHQ4 (1998).

[148] A. Boschetti, D. Bassi, E. Iacob, S. Iannotta, L. Ricci, and M. Scotoni, "Resonant photoacoustic simultaneous detection of methane and ethylene by means of a 1.63 μm diode laser," *Appl. Phys. B* **74**, 273-278 (2002).

[149] M. W. Sigrist, "Trace gas monitoring by laser-photoacoustic spectroscopy", *Infrared Physics & Technol.* **36**, 415-425 (1995).

[150] J. M. Lopez-Higuera, **"**Handbook of Optical Fibre Sensing Technology", *John Wiley & Sons New York* (2002).

[151] J. R. Stetter, W. R. Penrose, and S. Yao, "Sensors, chemical sensors, electrochemical sensors, and ECS," *J. Electrochem. Soc.* **150**, S11-S16 (2003).

[152] O. S. Wolfbeis, "Fiber-Optic Chemical and Biosensors" *Boca Raton, FL: CRC Press* (1991).

[153] S. Sudo, I. Yokohama, H Yasaka, Y. Sakai, and T. Ikegami, "Optical fiber with sharp optical absorption by vibrational-rotational absorption of C_2H_2 molecules", *Photonics Technol. Lett*. **2**, 128-131 (1990).

[154] W. Jin, G. Stewart, and B. Culshaw, "Prospects for fibre-optic evanescent-field gas sensors using absorption in the near-infrared", *Sens. and Act. B* **38-39**, 42-47 (1997).

[155] R. E. Dyoit and P.F. Schrank, "Self-locating elliptically cored fibre with an accessible guiding region", *Electron. Lett.* **18**, 980-981 (1982).

[156] T. S. Lee, N. A. George, P. Sureshkumar, P. Radhakrishnan, C. P. G. Vallabhan, and V. P. N. Nampoori, "Chemical sensing with microbent optical fiber," *Opt. Lett.* **26**, 1541-1543 (2001).

[157] J. Harrington, "A review of IR transmitting hollow waveguides", *Fiber Integr. Opt*. **19**, 211–227 (2000).

[158] S. Luo, Y. Liu, A. Sucheta, M. Evans, and R. Tassell, "Applications of LPG fiber optical sensors for relative humidity and chemical warfare agents monitoring," *Advanced Sensor Systems and Applications SPIE* 193-204 (2002).

[159] J. T. Remillard, J. R. Jones, R. D. Poindexter, C. K. Narula, and W. H. Weber, "Demonstration of a high-temperature fiber-optic gas sensor made with a sol-gel process to incorporate a fluorescent indicator," *Appl. Opt.* **38**, 5306-5309 (1999).

[160] C. Singh and B. Gupta, "Detection of gases with porous-clad tapered fibers", *Appl. Opt.* **34**, 1019-(1995).

[161] Y. L. Hoo, W. Jin, C. Z. Shi, H. L. Ho, D. N. Wang, and S. C. Ruan, "Design and modeling of a photonic crystal fiber gas sensor", *Appl. Optics* **42**, 3509-3515 (2003).

[162] G. Pickrell, W. Peng, and A. Wang, "Random-hole fiber evanescent wave gas sensing", *Opt. Lett.* **29**, 1476-1478 (2004).

[163] J. Lægsgaard, N. A. Mortensen, J. Riishede, and A. Bjarklev, "Material effects in air-guiding photonic bandgap fibers", *J. Opt. Soc. Am. B*. **20**, 2046-2051 (2003).

[164] G. Humbert, J. C. Knight, G. Bouwmans, P. S. J. Russell, D. P. Williams, P. J. Roberts, and B. J. Mangan, "Hollow core photonic crystal fibers for beam delivery", *Opt. Express* **12,** 1477-1484 (2004).

[165] G. J. Pearce, J. M. Pottage, D. M. Bird, P. J. Roberts, J. C. Knight, and P. S. Russell, "Hollow-core PCF for guidance in the mid to far infra-red", *Opt. Express* **13,** 6937-6946 (2005).

[166] J. D. Shephard, W. N. MacPherson, R. R. J. Maier, J. D. C. Jones, D. P. Hand, M. Mohebbi, A. K. George, P. J. Roberts, and J. C. Knight, "Single-mode mid-IR guidance in a hollow-core photonic crystal fiber", *Opt. Express* **13,** 7139-7144 (2005).

[167] J. D. Shephard, J. D. C. Jones, D. P. Hand, G. Bouwmans, J. C. Knight, P. St.J. Russell, B. J. Mangan, "High energy nanosecond laser pulses delivered single-mode through hollow-core PBG fibers", *Opt. Express* **12,** 717-723 (2004).

[168] F. Benabid, G. Bouwmans, J. C. Knight, P. St.J. Russell, and F. Couny, "Ultrahigh efficiency laser wavelength conversion in a gas-filled hollow core photonic crystal fiber by pure stimulated rotational Raman scattering in molecular hydrogen", *Phys. Rev. Lett.* **93**, 123903 (2004).

[169] F. Benabid, J. C. Knight, and P. S. J. Russell, "Particle levitation and guidance in hollow-core photonic crystal fiber", *Opt. Express* **10,** 1195-1203 (2002).

[170] J. Henningsen, J. Hald, and J. C. Peterson, "Saturated absorption in acetylene and hydrogen cyanide in hollow-core photonic bandgap fibers", *Opt. Express* **13**, 10475-10482 (2005).

[171] M. Wegmuller, M. Legré, N. Gisin, T. P. Hansen, C. Jakobsen, and J. Broeng, "Experimental investigation of the polarization properties of a hollow core photonic bandgap fiber for 1550 nm", *Opt. Express* **13,** 1457-1467 (2005).

[172] C. Peucheret, B. Zsigri, T. P. Hansen, and P. Jeppesen, "10 Gbit/s transmission over airguiding photonic bandgap fibre at 1550 nm", *Electron. Lett.* **41**, 27-29 (2005).

[173] International Telecommunication Union (ITU), *Recommendation G.694.1 - Spectral grids for WDM applications: DWDM frequency grid*, 2002.

[174] M. Poulin, C. Latrasse, N. Cyr, and M. Têtu, "An absolute frequency reference at 192.6 THz (1556 nm) based on a two-photon absorption line of rubidium at 778 nm for WDM communication systems", *Photonics Technol. Lett.* **9**, 1631-1633 (1997).

[175] M. A. Rowe, W. C. Swann, and S. L. Gilbert, "Multiple-Wavelength Reference Based on Interleaved, Sampled Fiber Bragg Gratings and Molecular Absorption", *Appl. Opt.* **43**, 3530-3534 (2004).

[176] D. Humphreys, "Saturated optogalvanic transition in krypton at 1564 nm", *Symposium on Optical Fiber Measurements SOFM 2000,* 25-28 (2000).

[177] K.O. Hill, Y. Fujii, D. Johnson and B. Kawasaki, "Photosensitivity in optical fiber waveguides: Application to reflection filter fabrication", *Appl. Phys. Lett*. **32**, 647-649 (1978).

[178] Y. Chung, "Tunable Etalon Filter", *European Patent* EP0568242, 1992.

[179] J. Tuominen, T. Niemi, and H. Ludvigsen, "Wavelength reference for optical communications based on a temperature-tunable silicon etalon", *Rev. Sci. Instrum.* **74**, 3620-3623 (2003).

[180] D. A. Humphreys and J. Howes, "Accurate wavelength calibration for optical spectrum analysers using an etalon calibration artifact", *Optical Fiber Measurement Conference OFMC'97* 72-75 (1997).

[181] C. N. Banwell and E. M. McCash, "Fundamentals of Molecular Spectroscopy: Introduction", *McGraw-Hill* (1994).

[182] Y. Awaji, K. Nakagawa, M. de Labachelerie, and M. Ohtsu, "Optical frequency measurement of the $H^{12}C^{14}N$ Lamb-dip-stabilized 1.5-μm diode laser", *Opt. Lett.* **20**, 2024-2026 (1995).

[183] M. de Labachelerie, K. Nakagawa, Y. Awaji, and M. Ohtsu, "High-frequency-stability laser at 1.5 μm using Doppler-free molecular lines", *Opt. Lett.* **20**, 572-574 (1995).

[184] P. S. Light, F. Couny, F. Benabid, and P. S. J. Russell, "Electromagnetically-induced transparency and saturable absorption in all-fiber devices based on acetylene-filled hollow-core PCF", *European Conference on Optical Communication ECOC'05,* Th4.5.6 (2005).

[185] S. Ghosh, J. E. Sharping, D. G. Ouzounov, and A. L. Gaeta, "Resonant optical interactions with molecules confined in photonic band-gap fibers", *Phys. Rev. Lett.* **94**, 093902 (2005).

[186] J. Henningsen and J.C. Petersen, "Reference wavelength standards for optical communication: extended C-band coverage with $^{13}C_2H_2$", *Optical Fibre Measurement Conference OFMC 2001* 183-187 (2001).

[187] Telcordia Technologies, *GR-1209-CORE - Generic requirements for passive optical components*, 2001.

[188] T. Ritari, J. Tuominen, J. C. Petersen, T. P. Hansen, and H. Ludvigsen, "Miniature wavelength references based on gas-filled photonic bandgap fibers", *European Conference on Optical Communication ECOC '04* Mo3.3.2 (2004).

[189] F. Benabid, F. Couny, J. C. Knight, T. A. Birks, and P. St. J. Russell, "Compact, stable and efficient all-fiber gas cells using hollow-core photonic crystal fibers", *Nature* **434**, 488-491 (2005).

ISBN 951-22-8298-4
ISBN 951-22-8299-2 (PDF)
ISSN 1795-2239
ISSN 1795-4584 (PDF)